



HAL
open science

Retrieving robust noise-based seismic velocity changes from sparse data sets: synthetic tests and application to Klyuchevskoy volcanic group (Kamchatka)

C Gómez-García, F. Brenguier, P. Boue, N. M. Shapiro, D V Droznin, S. Ya. Droznina, S. L. Senyukov, E. I. Gordeev

► To cite this version:

C Gómez-García, F. Brenguier, P. Boue, N. M. Shapiro, D V Droznin, et al.. Retrieving robust noise-based seismic velocity changes from sparse data sets: synthetic tests and application to Klyuchevskoy volcanic group (Kamchatka). *Geophysical Journal International*, 2018, 214 (2), pp.1218-1236. 10.1093/gji/ggy190 . hal-02928326

HAL Id: hal-02928326

<https://hal.univ-grenoble-alpes.fr/hal-02928326v1>

Submitted on 3 Sep 2020

HAL is a multi-disciplinary open access archive for the deposit and dissemination of scientific research documents, whether they are published or not. The documents may come from teaching and research institutions in France or abroad, or from public or private research centers.

L'archive ouverte pluridisciplinaire **HAL**, est destinée au dépôt et à la diffusion de documents scientifiques de niveau recherche, publiés ou non, émanant des établissements d'enseignement et de recherche français ou étrangers, des laboratoires publics ou privés.

**Retrieving robust noise-based seismic velocity changes
from sparse data sets: synthetic tests and application to
Klyuchevskoy volcanic group (Kamchatka)**

C Gómez-García, F. Brenguier, P. Boue, N. M. Shapiro, D Droznin, S Ya
Droznina, S. L. Senyukov, E. I. Gordeev

► **To cite this version:**

C Gómez-García, F. Brenguier, P. Boue, N. M. Shapiro, D Droznin, et al.. Retrieving robust noise-based seismic velocity changes from sparse data sets: synthetic tests and application to Klyuchevskoy volcanic group (Kamchatka). *Geophysical Journal International*, Oxford University Press (OUP), 2018, 214 (2), pp.1218-1236. 10.1093/gji/ggy190 . hal-02928326

HAL Id: hal-02928326

<https://hal.univ-grenoble-alpes.fr/hal-02928326>

Submitted on 3 Sep 2020

HAL is a multi-disciplinary open access archive for the deposit and dissemination of scientific research documents, whether they are published or not. The documents may come from teaching and research institutions in France or abroad, or from public or private research centers.

L'archive ouverte pluridisciplinaire **HAL**, est destinée au dépôt et à la diffusion de documents scientifiques de niveau recherche, publiés ou non, émanant des établissements d'enseignement et de recherche français ou étrangers, des laboratoires publics ou privés.

1 **Retrieving robust noise-based seismic velocity changes from**
2 **sparse data sets: synthetic tests and application to**
3 **Klyuchevskoy volcanic group (Kamchatka)**

4 C. Gómez-García^{1,6}, F. Brenguier², P. Boué², N.M. Shapiro^{3,4}, D.V. Droznin⁵,
5 S. Ya. Droznina⁵, S.L. Senyukov⁵ and E.I. Gordeev⁴

¹*Instituto de Ciencias de la Tierra Jaume Almera, CSIC, Lluís Solé i Sabarís s/n, E-08028 Barcelona, Spain*

²*Institut des Sciences de la Terre, Université Grenoble Alpes, F-38041 Grenoble cedex 9, France*

³*Institut de Physique du Globe de Paris, Paris Sorbonne Cité, CNRS, 1 rue Jussieu, F-75238 Paris cedex 05, France*

⁴*Institute of Volcanology and Seismology FEB RAS, 9 Piip Boulevard, Petropavlovsk-Kamchatsky,
Kamchatsky Region 683006, Russia*

⁵*Kamchatka Branch of the Geophysical Service, Russian Academy of Sciences, 9 Piip Boulevard,
Petropavlovsk-Kamchatsky, Kamchatsky Region 683006, Russia*

⁶*Now at Dublin Institute for Advanced Studies, Geophysics Section, 5 Merrion Square, Dublin 2, Ireland*

E-mail: cgomez@cp.dias.ie

6

7 **SUMMARY**

8

9 Continuous noise-based monitoring of seismic velocity changes provides insights into
10 volcanic unrest, earthquake mechanisms and fluid injection in the sub-surface. The stan-
11 dard monitoring approach relies on measuring travel time changes of late coda arrivals
12 between daily and reference noise-cross-correlations, usually chosen as stacks of daily
13 cross-correlations. The main assumption of this method is that the shape of the noise
14 correlations does not change over time or, in other terms, that the ambient-noise sources
are stationary through time. These conditions are not fulfilled when a strong episodic

15 source of noise, such as volcanic tremor, for example, perturbs the reconstructed Green's
16 function. In this paper we propose a general formulation for retrieving continuous time
17 series of noise-based seismic velocity changes without the requirement of any arbitrary
18 reference cross-correlation function. We perform synthetic tests in order to establish a
19 general framework for future applications of this technique. In particular, we study the re-
20 liability of velocity changes measurements versus the stability of noise cross-correlation
21 functions. We apply this approach to a complex dataset of noise cross-correlations at
22 Klyuchevskoy volcanic group (Kamchatka), hampered by loss of data and the presence
23 of highly non-stationary seismic tremor.

24 **Key words:** Seismic noise; Time series analysis; Volcano monitoring; Seismic interfer-
25 ometry; Coda waves.

26 1 INTRODUCTION

27 Noise-based monitoring techniques have been used extensively in the past decade for different applica-
28 tions. The observation of continuous seismic velocity changes proved to be useful for detecting crustal
29 seasonal changes (e.g., Sens-Schönfelder & Wegler 2006; Meier et al. 2010; Ugalde et al. 2014), co-
30 and post-seismic evolution of stress in fault areas (e.g., Brenguier et al. 2008a; Hobiger et al. 2012)
31 and, more recently, for studying the effects of fluid injection (e.g., Zhou et al. 2010; Ugalde et al. 2013)
32 and aseismic deformation transients (Hillers et al. 2015).

33 Estimation of temporal velocity changes in volcano interiors using seismic noise cross-correlation
34 has been shown to be an efficient method for early detection of volcanic unrest prior to eruptions at
35 Piton de la Fournaise Volcano, La Réunion (e.g., Brenguier et al. 2008b; Duputel et al. 2009). Although
36 precise eruption and eruption intensity forecasting is still a challenge, it has been demonstrated that
37 this method provides meaningful constraints on the location of oncoming eruptions (Obermann et al.
38 2013).

39 The most important step in noise-based monitoring is the reconstruction of Green's function (GF)
40 between two receivers from the correlation of ambient seismic noise (e.g., Shapiro & Campillo 2004;
41 Shapiro et al. 2005; Larose et al. 2006; Wapenaar et al. 2010; Campillo et al. 2011). If the noise sources
42 are evenly distributed over the Earth's surface, leading to an isotropic and equipartitioned wavefield at
43 the two station locations, the cross-correlation function (CCF) between these two stations converges
44 towards the GF (e.g., Roux et al. 2005; Wapenaar & Fokkema 2006). This is an ideal situation but, in

45 practice, noise sources are distributed irregularly leading to a partial reconstruction of the GF (Shapiro
46 et al. 2006).

47 For monitoring purposes, it is possible to retrieve temporal seismic velocity changes over a set
48 of repetitive in time noise cross-correlations, even with anisotropic distributions of noise sources, as
49 long as this distribution does not change too much over time (Hadziioannou et al. 2009). Moreover,
50 measuring travel time changes in the coda part of the noise cross-correlations makes velocity change
51 measurements less sensitive to noise source temporal changes (Sens-Schönfelder & Wegler 2006;
52 Wegler & Sens-Schönfelder 2007; Colombi et al. 2014). The standard monitoring approach relies
53 on measuring travel time changes of late coda arrivals between a daily and a reference noise-cross-
54 correlation, usually chosen as a stack of all daily cross-correlations. We assume that the measured time
55 delay from the coda waveform of noise cross-correlations ($d\tau$) is caused by a spatially homogeneous
56 relative velocity change, $d\nu/\nu$. Under this assumption, the relative delay time ($d\tau/\tau$) is constant and
57 independent of the lapse time at which it is measured: $d\tau/\tau = -d\nu/\nu$.

58 In different environments, and especially on volcanoes, the noise correlations can be altered by
59 strong episodic sources of noise as volcanic tremor, for example, that overlaps in frequency with more
60 stable microseismic noise. There is thus a problem with the definition of the reference function if the
61 sources are non-stationary (Sens-Schönfelder et al. 2014). Very strong non-stationary noise has been
62 described by Ballmer et al. (2013) and Droznin et al. (2015) in case of emission of low frequency
63 volcanic tremor, a typical feature of the unrest of many volcanoes and an important seismic source for
64 monitoring plumbing systems (e.g., Chouet 1996).

65 In this article, we describe a new generalized approach for retrieving continuous time series of
66 noise-based seismic velocity changes without the definition of an arbitrary reference CCF. Brenguier
67 et al. (2014) proposed the method used in this paper (Section 2). We detail the method carrying out
68 synthetic tests that allow us to evaluate the reliability of measured velocity changes in regard to the
69 level of stability of noise cross-correlation functions and the influence of temporary strong changes
70 (Section 3). Finally, we apply our procedure to a real dataset in Section 4. We choose the Klyuchevskoy
71 volcanic group (Kamchatka) as a case study where the recorded wavefield is dominated by strongly
72 localized volcanic tremor sources and is hampered by lose of data and the presence of highly non-
73 stationary seismic noise. This approach will be useful for improving noise-based seismic monitoring
74 at all scales in cases where noise sources are not stable in time.

75 **2 METHOD**

76 The standard approach for measuring continuous time series of noise-based seismic velocity changes
77 relies on measuring travel time differences between a set of noise cross-correlations at different dates

78 and a so-called reference cross-correlation. The reference CCF is usually defined as the stack of all
 79 cross-correlations for a given station pair at different days (Breguier et al. 2008b). Temporal changes
 80 of seismic velocities are then measured using a Moving Window Cross Spectral (MWCS) procedure
 81 between the daily and reference cross-correlation functions by measuring travel time changes along
 82 the coda part of the cross-correlation functions (Clarke et al. 2011).

83 Here, we propose a general formulation for retrieving continuous time series of velocity changes
 84 without the requirement of a reference stacked cross-correlation function. The novel procedure relies
 85 on measuring seismic velocity changes between all possible pairs of daily cross-correlation functions.
 86 An inversion step is further required to retrieve a continuous time series of daily seismic velocity
 87 changes (Breguier et al. 2014).

88 By considering (ccf_i) as a cross-correlation function that corresponds to day i , we can thus esti-
 89 mate a seismic velocity (ν_{ij}) change between day i and day j by applying the MWCS analysis to ccf_i
 90 and ccf_j :

$$\delta\nu_{ij} = \frac{\nu_j - \nu_i}{\nu_i} = \text{MWCS}(ccf_i, ccf_j) \quad (1)$$

91 $\delta\nu_{ij}$ is referred as a doublet measurement. This concept was used, initially, in pairs of microearthquakes
 92 (Poupinet et al. 1984). In a systematic manner, we can then estimate a velocity change between all of
 93 the pairs of daily cross-correlation functions for one given station pair. This constitutes the data vector
 94 of Equation (2):

$$\mathbf{d} = \begin{bmatrix} \delta\nu_{12} \\ \delta\nu_{13} \\ \delta\nu_{14} \\ \vdots \\ \delta\nu_{n-1n} \end{bmatrix} \quad (2)$$

95 where \mathbf{d} is of length $\frac{n \cdot (n-1)}{2}$, with n the number of daily cross-correlation functions.

96 Our final goal is to reconstruct the time series of daily velocity changes. We can define these
 97 velocity changes as $\delta\nu_i = \frac{\nu_i - \nu_{ref}}{\nu_{ref}}$, with ν_{ref} the reference velocity averaged along the entire studied
 98 time period. The series of velocity changes constitutes our model vector, \mathbf{m} , of Equation (3):

$$\mathbf{m} = \begin{bmatrix} \delta\nu_1 \\ \delta\nu_2 \\ \delta\nu_3 \\ \vdots \\ \delta\nu_n \end{bmatrix} \quad (3)$$

where \mathbf{m} is of length n , the number of daily cross-correlation functions.

The relation between \mathbf{d} and \mathbf{m} is given by:

$$\delta\nu_j - \delta\nu_i = \frac{\nu_j - \nu_i}{\nu_{ref}} = \frac{\nu_j - \nu_i}{\nu_i} \cdot \frac{\nu_i}{\nu_{ref}} = \delta\nu_{ij} \cdot \frac{\nu_i}{\nu_{ref}} = \delta\nu_{ij} \cdot (1 + \delta\nu_i) \quad (4)$$

Under the assumption that $\delta\nu_i$ and $\delta\nu_{ij}$ are small compared to 1 ($< 0.1\%$), we can write at the first order the direct linear relationship between \mathbf{d} and \mathbf{m} as $\delta\nu_{ij} = \delta\nu_j - \delta\nu_i$ or $\mathbf{d} = \mathbf{G}\mathbf{m}$, with \mathbf{G} being a sparse matrix of dimension $\left[\frac{n \cdot (n-1)}{2}, n\right]$:

$$\mathbf{G} = \begin{bmatrix} -1 & 1 & 0 & \dots & & \dots & 0 \\ -1 & 0 & 1 & 0 & \dots & & \vdots \\ -1 & 0 & 0 & 1 & 0 & \dots & \\ \vdots & & & & \ddots & & \vdots \\ 0 & \dots & & & \dots & 0 & -1 & 1 \end{bmatrix} \quad (5)$$

The assumption made above ($\delta\nu_i$ and $\delta\nu_{ij} < 0.1\%$) is necessary to apply our method. Temporal velocity changes ($\delta\nu_i$) are sensitive to transient stress changes (e.g., Niu et al. 2008) and the magnitude order of the seismic velocity changes depends on the level of applied stress in the medium. Some examples of typical magnitude orders of $\delta\nu_i$ estimations are $\sim -0.1\%$ in the Piton de la Fournaise volcano (Brenugier et al. 2008b; Obermann et al. 2013), $\sim -0.12\%$ due to the Tohoku-Oki earthquake (Brenugier et al. 2014), $\sim -0.15\%$ due to the Parkfield earthquake (Schaff 2012), $\sim -0.5\%$ due to the Nicoya Peninsula earthquake (Chaves & Schwartz 2016) or $\sim -0.8\%$ in Ruapehu volcano (Mordret et al. 2010).

The final time series of velocity changes (\mathbf{m}) is obtained by further inversion, using a classical Bayesian linear least square formulation (Tarantola 2005; details in Brenugier et al. 2014):

$$\mathbf{m} = (\mathbf{G}^t \mathbf{C}_d^{-1} \mathbf{G} + \alpha \mathbf{C}_m^{-1})^{-1} \mathbf{G}^t \mathbf{C}_d^{-1} \mathbf{d} \quad (6)$$

where \mathbf{C}_d is a covariance matrix of dimension $\left[\frac{n \cdot (n-1)}{2}, \frac{n \cdot (n-1)}{2}\right]$ that describes the Gaussian

115 uncertainties of the data vector \mathbf{d} . These values correspond to the estimated uncertainties of each $\delta\nu_{ij}$
 116 estimate, using the MWCS analysis.

117 \mathbf{C}_m is an a priori covariance matrix of dimension $[n, n]$ for model vector \mathbf{m} . The parameter α is
 118 a weighting coefficient. It is determined in a way that matrix $(\mathbf{G}^t \mathbf{C}_d^{-1} \mathbf{G})$ and $(\alpha \mathbf{C}_m^{-1})$ have approx-
 119 imately the same weight. Since α behaves as the amplitude of the inverse of the distribution \mathbf{C}_m , the
 120 larger the α , the less the model can change from one point to another point and, therefore, the lower
 121 the amplitude and smoother the final time series will be.

122 The values of \mathbf{C}_m describe for day i how $\delta\nu_i$ is correlated to $\delta\nu_j$ at day j :

$$C_{m_{ij}} = e^{\frac{-|i-j|}{2\beta}} \quad (7)$$

123 where β is the characteristic correlation length between the model parameters $\delta\nu$. A day, i , is
 124 more correlated with the β days before and after than with any others. For this reason, large values
 125 of β correspond to velocity change curves (long-term variations) that avoid short-term fluctuations,
 126 whereas small β values represent the opposite situation (short-term variations).

127 In Fig. 1 we compare the standard and the general approach. Even though the computing cost
 128 of the general formulation is higher than that of the standard approach, this formulation manifests
 129 several advantages. We can deal with irregular sampling in time of noise correlations; therefore, this
 130 technique is more efficient when the dataset is complex. Also, long-term or short-term trends are
 131 obtained directly from the inversion process rather than fitting the velocity change time series with
 132 polynomial functions, as in the standard approach (Breguier et al. 2008b).

133 In this work we consider station pairs independently to obtain single time series of velocity fluc-
 134 tuations but we can also invert several raypaths at the same time to achieve a more homogeneous and
 135 general trend of seismic velocity variations rather than averaging over different time series from dif-
 136 ferent station pairs. By concatenating doublet measurements from different station pairs for a global
 137 inversion, the robustness of retrieved velocity changes improves by minimizing the effect of missing
 138 data.

139 In the following, we describe synthetic tests to explicit the advantages and limits of that novel
 140 approach.

141 **3 SYNTHETIC TESTS**

142 In this section we analyze how the stability of noise-correlations influences the reconstruction of ve-
 143 locity change time series for different cases. Specifically, the causes that we want to study are:

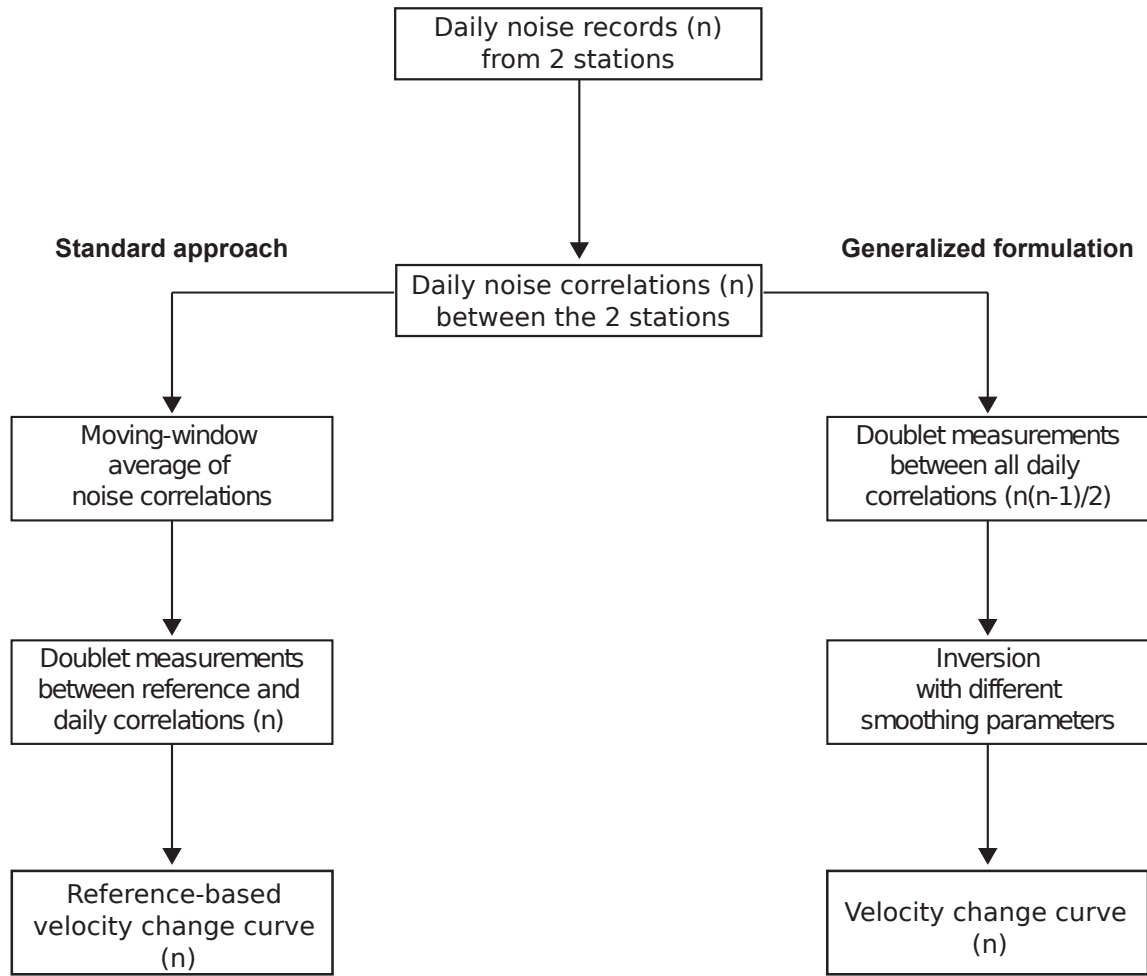


Figure 1. Workflow diagram showing the main steps of the standard approach and the general one. n is the number of days.

144 • Seasonal-type trends which produce long-term periodic-type velocity changes, i. e., long-term
 145 variations.

146 • Rapid transient changes similar to those produced as a result of an earthquake or a volcanic
 147 eruption. The effect of those changes in the noise correlations is the retrieval of a sudden velocity drop
 148 (short-term variations), corresponding to a permanent or almost permanent velocity change.

149 • Transient strong perturbations of the noise correlations due to a local source emission, such as the
 150 perturbation induced by episodic volcanic tremor (Droznin et al. 2015). The consequence is a sudden
 151 velocity drop and a sudden recovery, producing short and medium-term velocity fluctuations.

152 We use a synthetic test approach by artificially stretching noise cross-correlations in order to
 153 simulate synthetic velocity changes. We further degrade the quality of the dataset of noise cross-
 154 correlations by adding different levels of random noise in order to simulate unstable to stable noise
 155 cross-correlations. We then apply our novel method for reconstructing velocity changes and finally

156 compare the 'expected' and the 'reconstructed' time series of velocity changes. We also study the
 157 improvement of averaging the inverted times series of velocity changes for different station pairs.

158 The Pearson correlation coefficient (coherence) between two synthetic noise cross-correlations is
 159 used as a proxy for the quality of the associated doublet measurement and used to built the \mathbf{C}_d matrix
 160 of data weighting. The average of all Pearson correlation coefficients between all pairs of noise cross-
 161 correlations (CCFs) is referred as the coherence level. This value describes the level of added random
 162 noise by varying from 0 (totally incoherent noise CCFs) to 1 (no random noise added).

163 **3.1 Long-term periodic-type fluctuation test**

164 In this section we refer to velocity change measurements at a crustal scale using micro-seismic noise
 165 correlations in the frequency range from 0.1 to 1 Hz. However, this approach can be extended to other
 166 frequency domains and sources of seismic noise.

167 By stretching a single arbitrary CCF with different daily velocity changes (referred as expected
 168 velocity changes henceforth), we simulate daily synthetic CCFs. Fig. 2, right panel shows the expected
 169 velocity changes that we apply and that simulate long-term periodic-type velocity changes. The other
 170 panels of Fig. 2 show examples of synthetic CCFs with different levels of noise. The different panels of
 171 synthetic CCFs are associated with a coherence level (referred as *coh* in the figures), that is a measure
 172 of the level of added random noise. By adding random noise we are 'hiding' the original time series
 173 of velocity changes that we want to reconstruct after inversion, i. e., the 'expected' velocity changes.

174 We obtain the data vector of velocity changes, \mathbf{d} , by applying a MWCS analysis between all possi-
 175 ble pairs of CCFs. For n daily cross-correlation functions, we estimate $\frac{n(n-1)}{2}$ doublet measurements.
 176 We measure doublets in windows of 10 s centered between the direct surface-wave arrival time and
 177 a lapse time of 70 s in the coda. Moving windows are overlapped by 80 %. We finally perform the
 178 inversion for retrieving daily velocity changes (vector \mathbf{m}). As we are studying long-term variations,
 179 we use a large β values to retrieve $d\nu/\nu$ series, $\beta = 1000$, while α decreases with the coherence level,
 180 from $\alpha = 5000$ to $\alpha = 100$.

181 In Fig. 3 we compare the reconstructed time series of velocity changes obtained from the synthetic
 182 CCFs of Fig. 2 with the expected one. The more noise we add, the less coherence level we have and
 183 the more the reconstructed time series of velocity changes differ from the expected velocity changes.

184 We test three different levels of expected velocity changes (Fig. 4a) to achieve the final time series
 185 of velocity changes. The peak amplitude of the expected velocity change curve 1 is 0.001 %, while
 186 expected velocity change curves 2 and 3 present peak amplitudes of 0.005 % and 0.01 %, respectively.
 187 For Figs. 2 and 3 we use the expected velocity curve 3.

188 Fig. 4b shows the correlation coefficients between the reconstructed and the expected time series

189 as a function of the coherence levels, for the three different expected velocity changes. By considering
 190 greater velocity change amplitudes (expected velocity change curve 3), we achieve higher similarity
 191 between the reconstructed time series of velocity changes and the expected ones, for the same level of
 192 noise.

193 To simulate the averaging of inverted time series of velocity changes over different station pairs,
 194 we build different station pairs with synthetic stretched cross-correlation data. We apply the same
 195 velocity change stretching procedure but with different random noise to simulate different synthetic
 196 station pairs. We use the expected velocity change curve 3 and a fixed high level of noise ($coh = 0.06$)
 197 to simulate up to 50 different synthetic station pairs. After obtaining the 50 reconstructed velocity
 198 change curves, we average them to study the improvement. N_{sta} is the number of averaged curves of
 199 reconstructed velocity changes.

200 Fig. 5a shows higher correlation between time series (Fig. 5b) with higher number of averaged
 201 curves, N_{sta} . With this low coherence level we can retrieve a correlation coefficient between the in-
 202 verted and expected velocity change curves of more than 0.9 for $N_{sta} = 50$ and for $N_{sta} = 20$ we
 203 already reach a correlation coefficient of 0.7. Fig. 5b shows the averaged curve for $N_{sta} = 50$ and
 204 the expected velocity change curve 3. In general, it is thus recommended to average seismic velocity
 205 changes over at least 20 station pairs when the noise cross-correlations are so unstable. Although Fig.
 206 5a shows a correlation coefficient of 0.22 for $N_{sta} = 1$, in Fig. 3 we show a greater correlation coeffi-
 207 cient, 0.41, for the same coherence level, $coh = 0.06$, because we picked one of the best examples to
 208 show.

209 With this test we have studied how our method resolves the effects of a seasonal-type trend. To
 210 recover long-term periodic-type fluctuations, we choose a high β value, $\beta = 1000$, while depending
 211 on the coh of the CCFs, we use different values for α , choosing lower values for lower coh , to fit better
 212 the expected velocity change curve. With the use of three different expected velocity change curves,
 213 we also have seen that the reconstructed time series of velocity changes is closer to the expected one
 214 when the velocity change amplitudes to retrieve are greater. On the other hand, it is also important to
 215 note that, although there is a great improvement when averaging over different station pairs (Fig. 5a,
 216 from a correlation of 0.22 for $N_{sta} = 1$ to 0.87 for $N_{sta} = 50$, increasing then the correlation by a
 217 factor of 3.9), the reconstructed velocity changes will remain underestimated (there is no convergence
 218 to 1, Fig. 5a, and the amplitude of the reconstructed time series of velocity changes for $N_{sta} = 50$
 219 is one magnitude order smaller than the expected velocity changes, Fig. 5b), probably due to an edge
 220 effect of the time series. In case of CCFs with low coh , it is recommended to average seismic velocity
 221 changes over several station pairs, at least over 20 in case of very unstable CCFs.

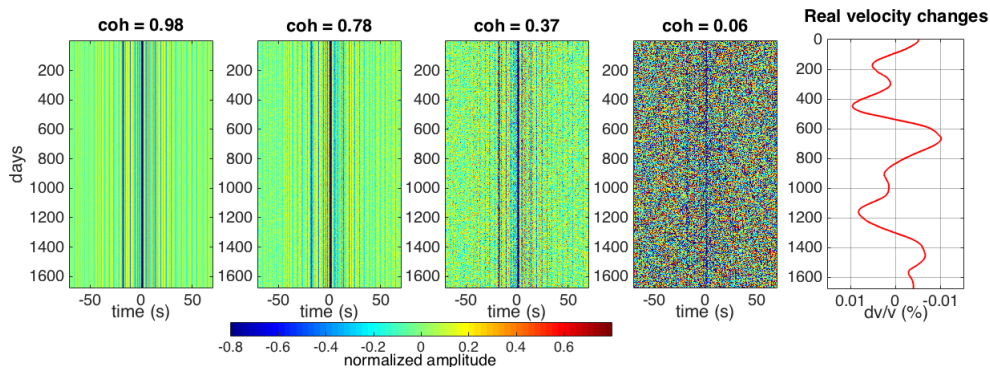


Figure 2. Examples of synthetic stretched CCFs with different levels of random noise. The coherence level (coh) is on top of each figure. On the right, expected velocity changes applied to stretch the CCFs (red curve).

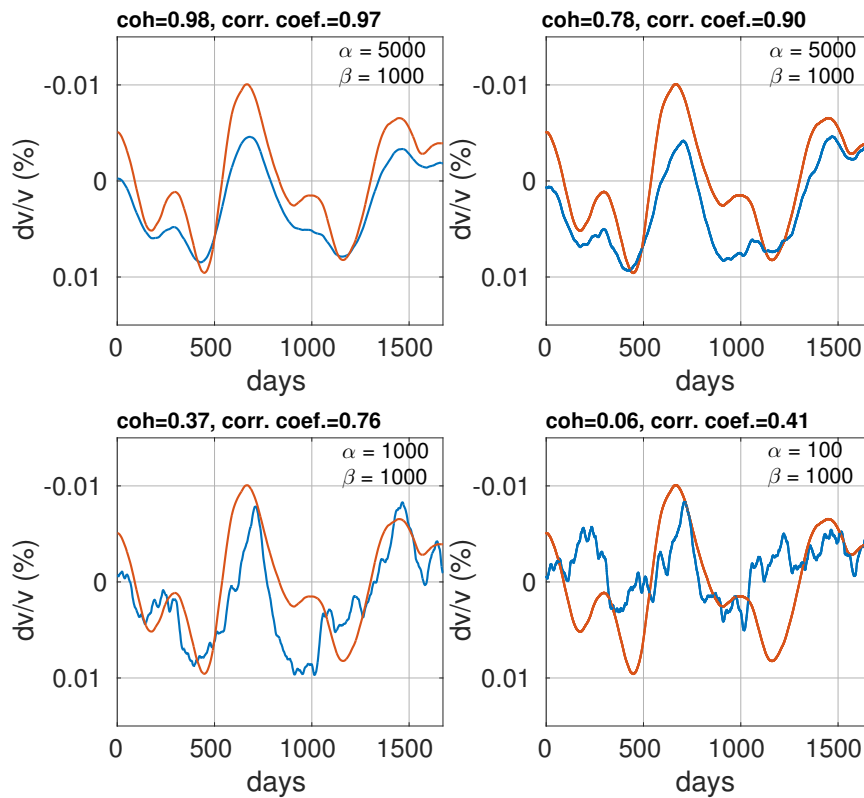


Figure 3. Reconstructed velocity change time series (blue curves) vs. the expected velocity changes (red curve) for different coherence levels. Correlation coefficients between both curves on top of each figure.

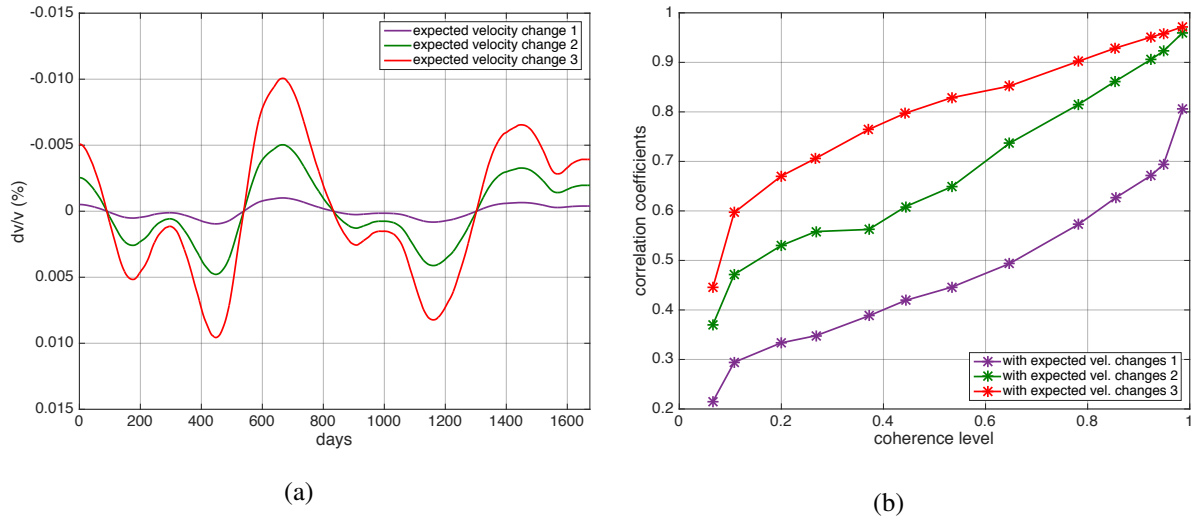


Figure 4. (a) Expected velocity change curves used in the long-term periodic-type fluctuation test. (b) Convergence curves of the coherence levels and the correlation coefficients between the reconstructed velocity change time series and the different expected velocity changes.

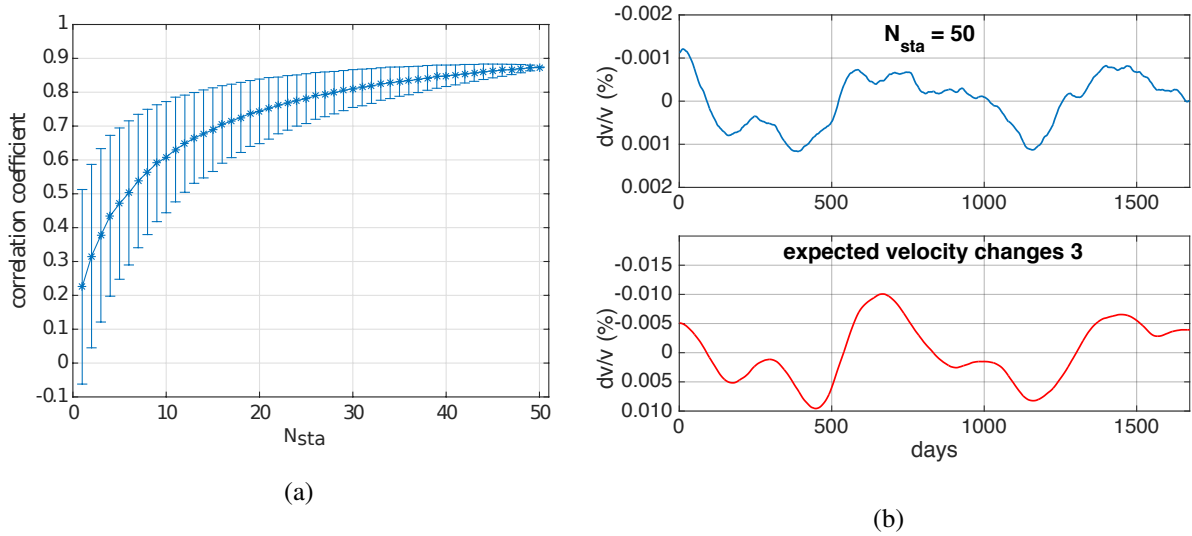


Figure 5. For a coherence level = 0.06 and the expected velocity change curve 3: (a) Correlation coefficients between the reconstructed velocity change time series and the expected velocity changes 3 as a function of the number of averaged curves of reconstructed velocity changes, N_{sta} . Associated standard deviations in blue bars. (b) Reconstructed velocity change time series for $N_{sta} = 50$ (blue) and the expected velocity change curve 3 (red).

222 3.2 Velocity drop test

223 To test the reconstruction of an abrupt, rapid change of velocity, similar to the effect of an earthquake
 224 (e.g., Brenguier et al. 2008a), we add a Heaviside step function with a velocity change of 0.05 %, to
 225 the previous expected velocity change curve 3 (Fig. 6, red curve), referred as the drop curve in this
 226 section

227 As we are interested in recovering the drop, we use another coefficient to study the similarity
 228 between the reconstructed time series and the drop curve instead of using the Pearson correlation
 229 coefficient. To estimate the quality of the reconstructed drop, we measure the difference between the
 230 mean velocity changes after and before the drop:

$$diff = \left(\frac{d\nu}{\nu} \right)_{after\ drop} - \left(\frac{d\nu}{\nu} \right)_{before\ drop} \quad (8)$$

231 We compute $diff$ for both the reconstructed velocity change curve and the expected drop curve.
 232 We then estimate the quality of the reconstructed drop by the ratio:

$$Q_{drop} = \left| \frac{diff_{reconstructed\ velocity\ change\ curve}}{diff_{drop\ curve}} \right| \quad (9)$$

233 Q_{drop} is 1 when perfectly reconstructed, and < 1 otherwise. In this test, we invert for time series of
 234 velocity changes by using a small β to obtain short-term variations, $\beta = 5$ and we avoid a smoothing
 235 factor ($\alpha \approx 0$).

236 Fig. 6 shows the retrieved drops for several examples of different coherence levels. As the level of
 237 noise increases (coh decreases), the drop in the reconstructed time series of velocity changes becomes
 238 smaller until it almost disappears (when the coherence level is nearly zero).

239 Fig. 7 shows the convergence of Q_{drop} for different coherence values of the synthetic cross-
 240 correlations.

241 We also study the improvement of averaging the reconstructed velocity change curves over differ-
 242 ent station pairs. For a fixed coherence level of 0.37, we study the convergence of the retrieved drop by
 243 increasing N_{sta} (Fig. 8a). Interestingly, by averaging more reconstructed velocity changes, we smooth
 244 the sharp short-term fluctuations while the recovered drop remains the same. We also estimate the
 245 increasing Signal to Noise Ratio (SNR) associated with the increasing number of averaged synthetic
 246 functions, N_{sta} , as:

$$SNR = \frac{level\ of\ recovered\ drop}{rms(averaged\ \frac{d\nu}{\nu}\ curve)} \quad (10)$$

247 with $\text{rms}(\text{averaged } \frac{dv}{v} \text{ curve})$ being the root mean square of velocity change mean curve for each
 248 N_{sta} (Fig. 8a).

249 A way to increase the coherence between CCFs and, therefore, to improve the temporal resolution
 250 of the velocity change measurements, is the use of denoising methods such as Curvelet filtering (Stehly
 251 et al. 2015) or Wiener filtering. We applied a FIR Wiener filter to our CCFs without obtaining a great
 252 improvement in the reconstructed velocity changes, probably because this technique affect only to the
 253 amplitude of the frequency spectrum whereas the method presented in this article only uses the phase
 254 of the signal.

255 For a coherence level of 0.37 and $N_{sta} = 50$, we get a Q_{drop} of 0.6 and a SNR of 38 (Figs 8a
 256 and 8b). Again, it is interesting to note that, for highly unstable correlations (e.g., $\text{coh}=0.37$), averaging
 257 over different station pairs will not improve the value of the level of the velocity drop that will
 258 remain underestimated. Averaging over different receiver pairs will however improve the SNR of the
 259 recovered velocity changes and thus allow a better estimate of the timing of the velocity drop.

260 To summarize, the reason for this test was to check the effect of a sudden change in the structure,
 261 similar to the effect of a volcanic eruption or an earthquake. Simulating a transient change, we can
 262 infer short-term velocity fluctuations. We used $\beta = 5$, avoiding the smoothing ($\alpha \approx 0$), in order to
 263 study just the effect of the velocity drop with our method. The lower the coh of the CCFs considered,
 264 the smaller the velocity drop in the reconstructed time series of velocity changes. We have seen that
 265 this velocity drop remains underestimated, even averaging over several station pairs, although the
 266 improvement associated to the SNR of the reconstructed velocity changes allows us to set better when
 267 the velocity drop happens.

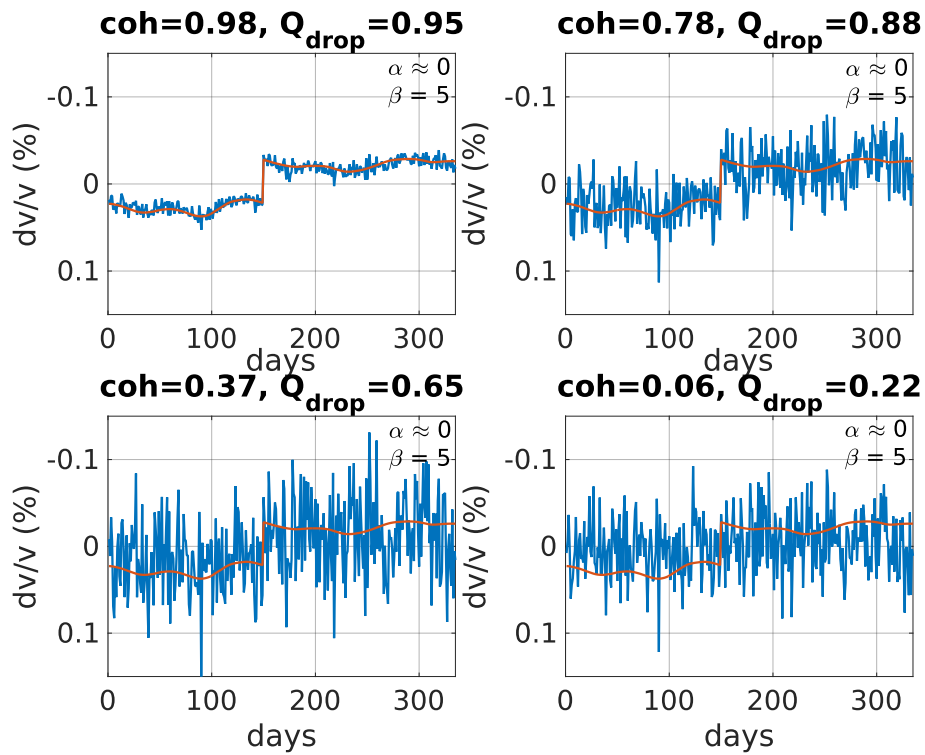


Figure 6. Reconstructed velocity change time series (blue curves) vs. the drop curve (red curve) for different coherence levels. Q_{drop} on top of each figure.

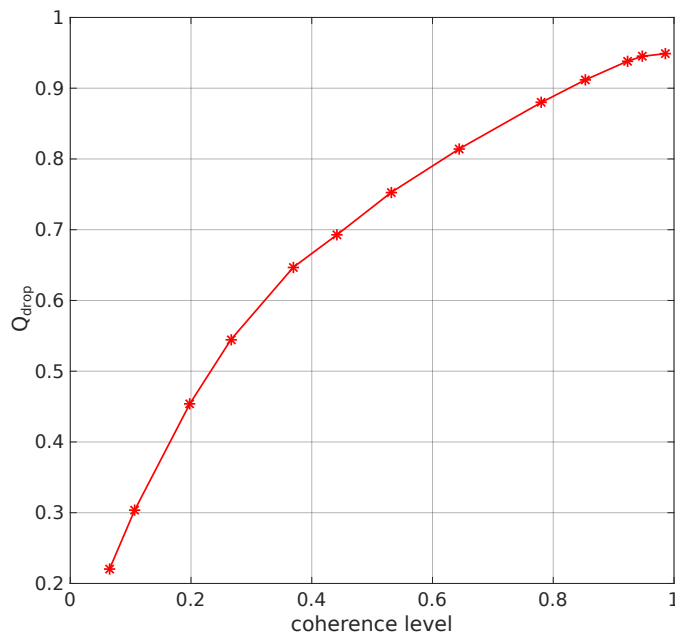


Figure 7. Convergence curve between the coherence levels and the percentage of the recovered drop.

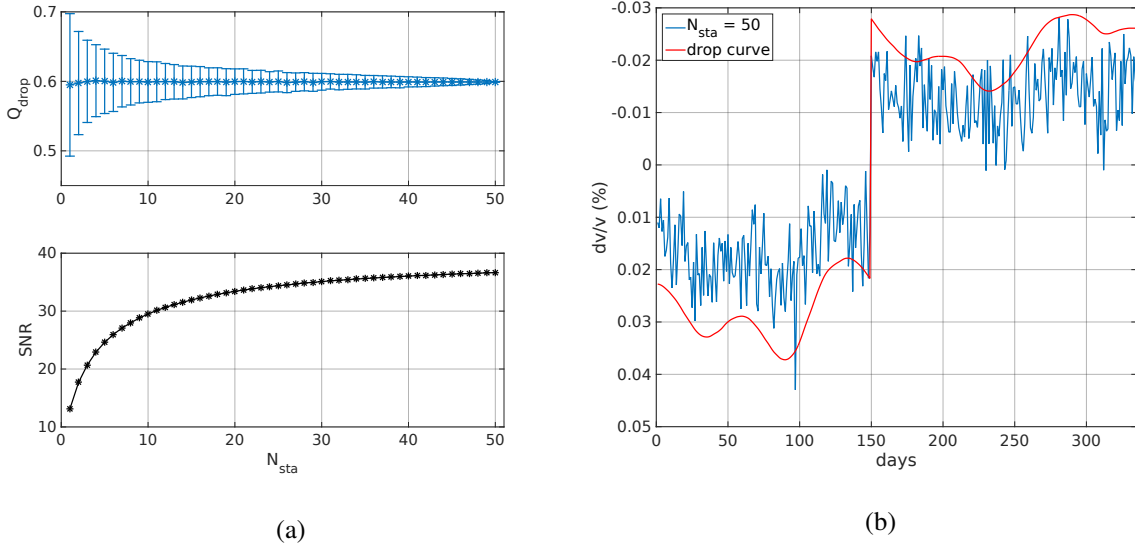


Figure 8. For a coherence level = 0.37: (a) Percentage of recovered drop (associated standard deviations in blue bars) and signal-to-noise ratio (SNR) (black curve) as a function of the number of synthetic averaged functions (N_{sta}). (b) Reconstructed velocity change time series for $N_{sta} = 50$ and drop curve.

268 3.3 Transient noise perturbation test

269 In this test we study the effect of an episodic strong change in the noise-correlation shape induced by a
270 strong noise source change, e.g., a passing storm or a episodic volcanic tremor. This last situation has
271 been described by Ballmer et al. (2013) and Droznin et al. (2015) in case of noise-correlations affected
272 by the occurrence of low-frequency volcanic tremor. We herewith test the ability of our method to
273 recover robust velocity changes in this situation.

274 To compute the synthetic stretched CCFs, we consider two real normalized CCFs, one during a
275 non-tremor period (C_1) and the other during a tremor period (C_2). Basically we consider C_1 as the
276 true GF and C_2 as a pure tremor-related bias. With both, we make two new averaged correlations:
277 $C_3 = 0.8 \times C_1 + 0.2 \times C_2$ and $C_4 = 0.8 \times C_2 + 0.2 \times C_1$, corresponding to a calm period (C_3) and to
278 a tremor period (C_4), respectively. We concatenate N_1 correlations C_3 , N_2 correlations C_4 and again
279 N_1 correlations C_3 , N_1 and N_2 being random numbers of daily CCFs. Then, we stretch the CCFs and
280 add different levels of random noise to these correlations in the same way than in previous tests.

281 Fig. 9a is an example of synthetic stretched CCFs with a certain level of random noise ($coh =$
282 0.54). We see clearly the differences in the shape of CCFs corresponding to a calm period, C_3 (from
283 $n = 1$ to $n = 30$ and from $n = 90$ to $n = 120$ in Fig. 9a), and to a tremor period, C_4 (from $n = 30$ to
284 $n = 90$ in Fig. 9a). Fig. 9b is the associated correlation coefficient matrix of Fig. 9a which represents
285 all Pearson correlation coefficients between all pairs CCFs. We observe the lower correlation between
286 CCFs of the tremor period comparing with the calm periods.

287 Fig. 10 shows some examples of the resulting reconstructed time series of velocity changes for
 288 the maximum coherence level of 0.85 and for some lower ones, where the coherence level decreases
 289 due to the increased level of random noise in the synthetic CCFs. We also plot the expected velocity
 290 curve for comparison. In the cases of a high coherence level, we observe a double velocity drop in the
 291 recovered synthetic velocity change curves (between days 30 and 90) due to the three different parts
 292 of the synthetic functions, i.e., the first N_1 days (calm period), the next N_2 days (tremor period) and
 293 the last N_1 days (calm period again) (Fig. 9). We explain this double velocity drop by looking at the
 294 correlation coefficient matrix (Fig. 9b). Since the correlation coefficients of the noise CCFs between
 295 the calm and the tremor period are very low (Fig. 9b), our method treats these data segments separately
 296 and thus generates this baseline difference between the two periods. Therefore, these artificial velocity
 297 drops are artefacts from our method. The double velocity drop observed in the reconstructed time
 298 series is hidden when the level of noise increases.

299 Even more interesting, when we increase the number of inverted synthetic time series of velocity
 300 changes for a low coherence value to study the improvement associated with averaging over different
 301 station pairs (Fig. 11a), we see clearly the improvement in the similarity between the inverted curves
 302 and the expected one (Fig. 11b). This is because only C_1 , the medium, is coherent and the noise source
 303 perturbation is not seen the same way by all receiver pairs. This means that for some station pairs, the
 304 double velocity drop induced by the tremor has, sometime, opposite sign which, simply, cancels out
 305 while summing over different receiver pairs.

306 We have tested in this subsection the effect of a transient and sudden local source emission, pro-
 307 ducing short to medium-term fluctuations. Since we are interested on evaluating the sudden velocity
 308 drop and sudden recovery in the reconstructed time series of velocity variations, we consider $\beta = 5$
 309 and $\alpha \approx 0$, as in the previous test. We have observed artificial velocity drops produced by our method,
 310 visible only when the *coh* of the CCFs is high and hidden with low *coh*.

311 In conclusion, there are two approaches in the situation of strong noise perturbations. In case the
 312 coherence level between the noise CCFs is high, it might worth correcting for the artificial baseline
 313 difference after the inversion to retrieve proper velocity changes. When the coherence is low, the only
 314 way to retrieve a proper velocity change curve is to average over sufficient station pairs (50 in that
 315 example).

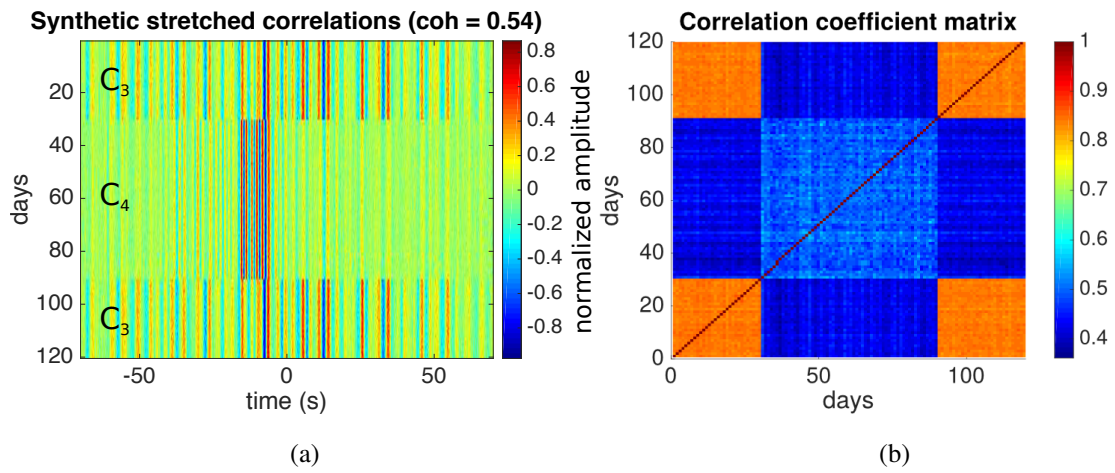


Figure 9. (a) Example of a normalized synthetic stretched CCFs of the tremor test with a random level of noise (shown for a coherence level between CCFs of 0.54). (b) Correlation coefficient matrix associated to the doublets.

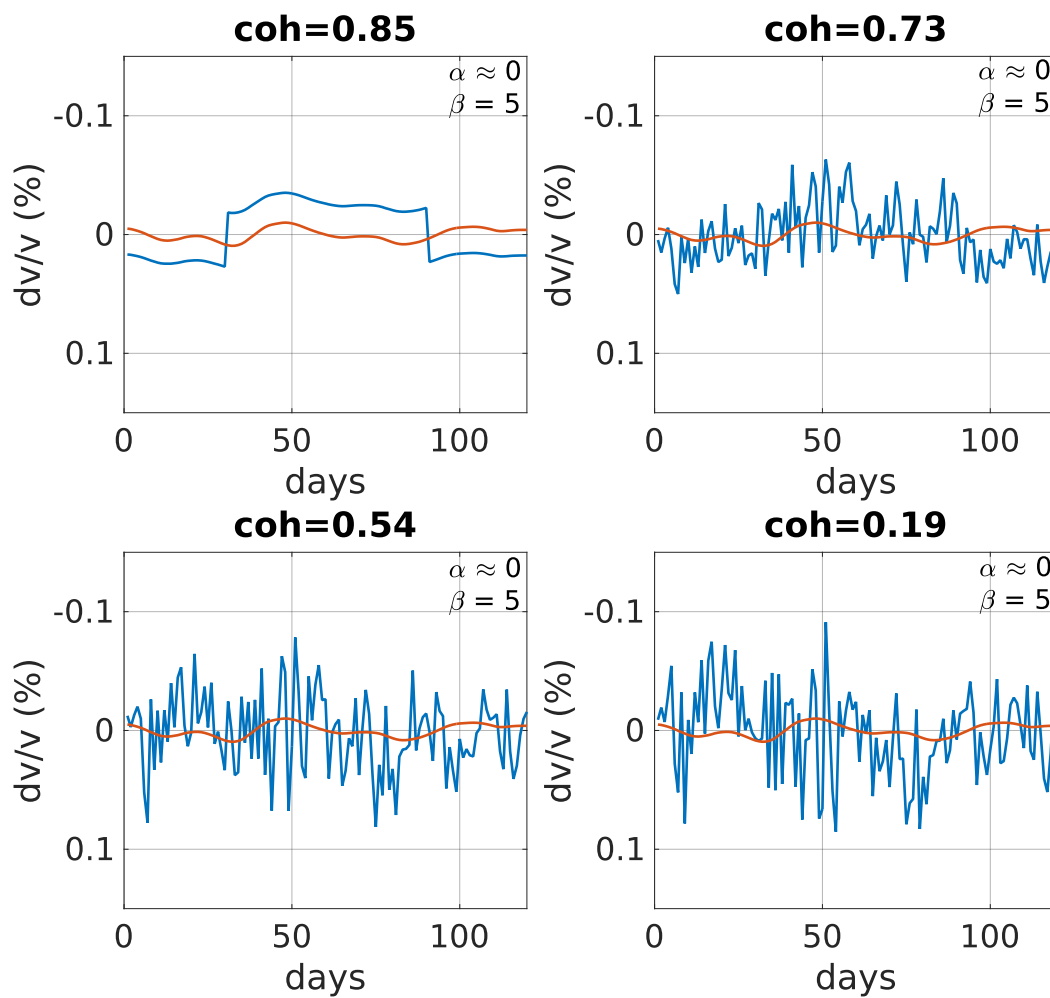


Figure 10. Synthetic velocity change time series (blue curves) vs. the expected velocity changes (red curve) for different coherence levels.

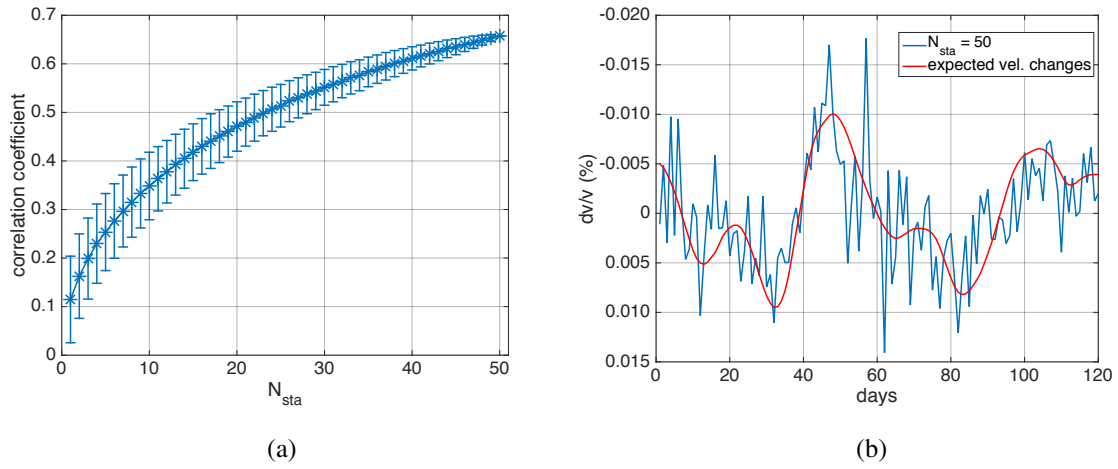


Figure 11. For a coherence level = 0.54: (a) Correlation coefficients between synthetic velocity change curves and the stretching curve as a function of the number of synthetic averaged functions (N_{sta}). (b) Reconstructed velocity change time series for $N_{sta} = 50$ compared to the expected velocity changes (red curve).

316 **4 APPLICATION TO REAL DATA**

317 With synthetic tests, we have established a general framework to identify and interpret long-term
318 periodic-type velocity changes from seasonal-type trends, rapid velocity drops, due to transient changes,
319 and sudden velocity drop and recovery as an effect of transient and sudden local source emissions. We
320 have analyzed the effect of the regularization parameters and the averaging over station pairs for the
321 three different cases. Now, we apply the method to a complex dataset of noise cross-correlations at
322 Klyuchevskoy volcanic group (Kamchatka), hampered by lose of data and the presence of highly
323 non-stationary seismic tremor.

324 **4.1 Klyuchevskoy volcanic group**

325 The Klyuchevskoy volcanic group (KVG), located in Kamchatka, is one of the most active clusters
326 of subduction-zone volcanoes in the world, where the annual rate of explosive eruptions is three to
327 five (Schneider et al. 2000). The KVG has an averaged extension of 70 km and 13 stratovolcanoes. It
328 includes active volcanoes such as Klyuchevskoy, Krestovsky, Ushkovsky, Bezymianny and Tolbachik.
329 The Klyuchevskoy Volcano, the most outstanding volcano with 4750 m high, is associated with the
330 emission of basaltic and basaltic-andesitic lavas and it has a mean eruptive rate of $1 \text{ m}^3 \text{ s}^{-1}$ over the
331 last 10 kyr (Fedotov et al. 1987). Two other active volcanoes, Shiveluch and Kizimen, are located only
332 60 kilometers north and south, respectively, of KVG. This cluster of volcanoes is located off the edge
333 of a tectonic junction: the Pacific Plate is subducting down the Aleutian Trench and also moving under
334 the Okhotsk Plate. The high volcanic activity is also a consequence of the Hawaii–Emperor Seamount
335 chain that terminates in the Kuril–Kamchatka Trench. Geodynamic models that have been proposed
336 to explain the exceptional activity of the KVG include fluid being released from the thick, highly
337 hydrated Hawaii–Emperor Seamount crust (Dorendorf et al. 2000), mantle flow around the corner of
338 the Pacific plate (Yogodzinski et al. 2001), and recent detachment of a portion of the subducting slab
339 (Levin et al. 2002; Levin et al. 2005).

340 The volcanic activity of the KVG leads to the generation of strong volcanic tremors (Gordeev et
341 al. 1990) with sources located very close to the surface and at depth near the crust mantle boundary
342 (Shapiro et al. 2017a) which spoil the ambient noise cross-correlations. We use the information of
343 Droznin et al. (2015) and Soubestre et al. (2017) about detection of these signals and about location of
344 their sources in Klyuchevskoy volcanic group to recover seismic velocity fluctuations in this region,
345 since we use the same dataset of noise cross-correlations as well.

346 The particular tectonic settings surrounding KVG and its strong eruptions with high seismic ac-
347 tivity (e.g. Senyukov et al. 2009; Zharinov & Demyanchuk 2009; Ozerov et al. 2013) enable many

348 seismic tomographic surveys (e.g. Slavina et al. 2012; Koulakov et al. 2013; Lees et al. 2013) and
349 receiver function analysis to study the internal structure of the KVG (Nikulin et al. 2010).

350 Tomographic studies on the KVG reveal a extremely high V_p/V_s ratio (up to 2.2), below 25 km
351 deep. This feature can acts as a channel which brings deep mantle materials from the mantle to the
352 bottom of the crust and is responsible for all volcanic activity in the KVG (Koulakov et al. 2013).

353 Our study period goes from January 2009 to July 2013 in which both the Klyuchevskoy and the
354 Tolbachik volcanoes erupted. From the Klyuchevskoy volcano, two eruptions took place. The first
355 one started in June 2008 and the volcanic activity ceased at the end of January 2009. The second
356 Klyuchevskoy eruption goes from July 2009 to December 7, 2010. Spatterings of hot magma started
357 on August 2, 2009. The summit eruption activity were characterized by weak ash emissions (less than
358 300 m of height) although in 2010 the ash emissions were stronger (9 km of height). The eruption
359 decreased at the end of 2010. All the recorded Klyuchevskoy summit eruptions are characterized by
360 a gradual growth of activity (Senyukov 2013). A detailed analysis of records of volcanic tremors has
361 been used by Soubestre et al. (2017) to identify two different stages of the 2009-2010 Klyuchevskoy
362 eruption with the stronger second stage starting approximately in June 2010.

363 The last eruption is the fissure eruption of the Tolbachik volcano (2012-2013). The 2012-13 Tol-
364 bachik eruption starts on November 27, 2012 corresponding to an eruptive tremor (Fig. 16) due to
365 a first magma migration (Caudron et al. 2015). The Tolbachik regional zone of cinder cones is 900
366 km^2 in size and 70 km long. Before last eruption (2012-2013), historical eruptions in Tolbachik zone
367 occurred in 1740, 1941 and 1975-1976 (Gordeev et al. 2013).

368 The three eruptions are characterized by emissions of seismic tremors (Gordeev et al. 1990;
369 Droznin et al. 2015; Shapiro et al. 2017a).

370 **4.2 Data**

371 We use continuous records from a total of 18 three-component seismic stations (Fig. 12) of the seis-
372 mic network deployed by the Kamchatka Branch of the Geophysical Service (KBGS) of the Russian
373 Academy of Sciences (Chebrov et al. 2013). Every component of the stations presents a CM-3 short
374 period sensor. We analyze data recorded continuously between 1 January 2009 and 7 July 2013.

375 Records are digitalized at 128 samples per seconds and downsampled to 8 samples per second.
376 Cross-correlations are calculated in 24-h long segments. We pre-process the continuous records fol-
377 lowing the method described by Bensen et al. (2007). We choose a spectral band between 0.08 – 0.7
378 Hz because, after 0.7 Hz, the correlations are too much affected by volcanic tremor correlation sig-
379 nals. After whitening, 1-bit normalization suppresses high-amplitude data, such as earthquake signals,
380 and emphasizes low-amplitude data, such as ambient seismic vibrations. Volcanic tremors still act as

381 potential biasing signals perturbing the reconstructed GF, after reducing persistent signals from local-
382 ized sources with pre-processing. Then, we compute daily cross-correlation functions for all possible
383 station pairs. We work with coda waves of daily CCFs between the vertical-component records of the
384 station pairs (Rivet et al. 2014).

385 For passive monitoring techniques, both the continuity of the records and the good quality of data
386 are important. For this reason, we do first a quality check of the daily cross-correlation functions for
387 each possible seismic station pair, 209 pairs in total. We visually inspect all CCFs of each station
388 pair to rank them in different groups according to the quality of the recordings. Taking into account
389 the continuity and regularity over time of the CCFs where coda waves are clearly distinguished, we
390 consider three quality groups, from best to worst: A, B and C. We can apply our method to the CCFs
391 of the station pairs ranked in groups A and B but not to those of group C.

392 We work with station pairs ranked in group A, there are 23 in total. Fig. 13 shows an example of
393 daily CCFs computed for a station pair ranked in group A with its associated correlation coefficient
394 matrix. The periods with highest correlation coefficients correspond to the first two-thirds of 2010
395 and to 2013. While most of the station pairs of the group A are in the vicinity of Klyuchevskoy and
396 Tolbachik volcanoes, three station pairs (from stations BDR, SMK and SRK) are farther away from the
397 rest, in the vicinity of the Shiveluch volcano (Fig. 12). Because of this, in our study we separate these
398 three stations near Shiveluch from the others. By the MWCS analysis, we compute all the doublets for
399 the 23 station pairs.

400 Figs 14 and 15 show correlation coefficient matrices for each station pair ranked with A. We can
401 see different patterns in correlation coefficients if we compare the main group of station pairs (Fig. 14)
402 with the northern group (Fig. 15). All pairs show a strong correlation in the second half of 2010 and
403 in 2013, matching with the ongoing Klychevskoy and Tolbachik eruptions (Droznin et al. (2015), fig.
404 5), respectively. Highest correlation values are observed between the stations of the main group (Fig.
405 14).

406 Daily averaged levels of tremors are shown in Fig. 16, determined by the KBGS operators. The
407 strongest tremor activities of both volcanoes also match with the highest correlation coefficients be-
408 tween CCF (Fig. 14).

409 Before the inversion, we reject the doublets where the associated correlation coefficients (Figs 14
410 and 15) are smaller than 0.3. Thereby, we ensure the recovered temporal velocity variation curves tend
411 towards zero for days with bad quality recordings.

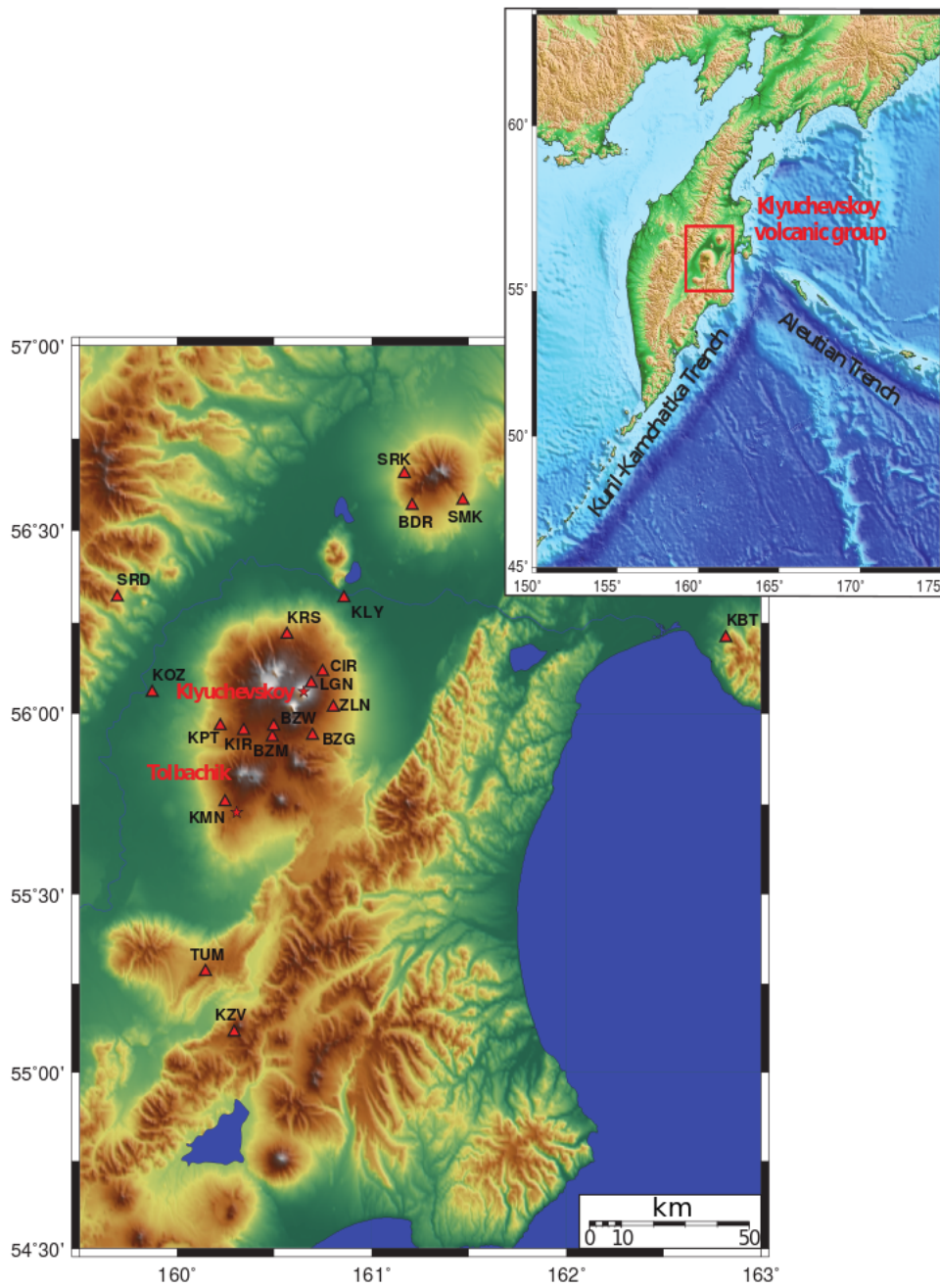


Figure 12. Topographic map of the Klyuchevskoy group of volcanoes in Kamchatka peninsula with positions of seismic stations. Red starts are the eruptive centres of the 2009-2010 Klyuchevskoy and of the 2012-2013 Tolbachik volcanoes.

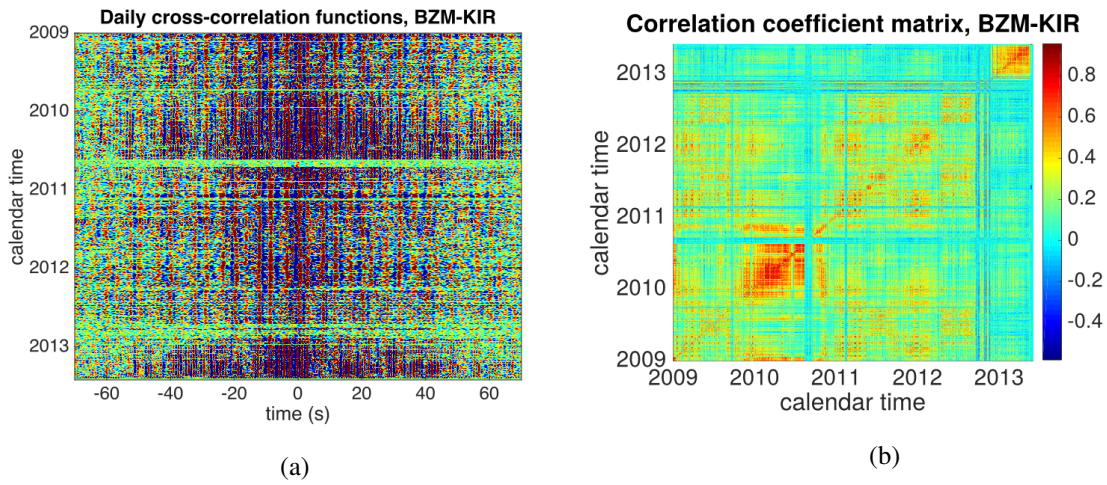


Figure 13. (a) Daily CCF computed from station pair BZM-KIR. (b) Correlation coefficient matrix associated to the doublets of the station pair BZM-KIR.

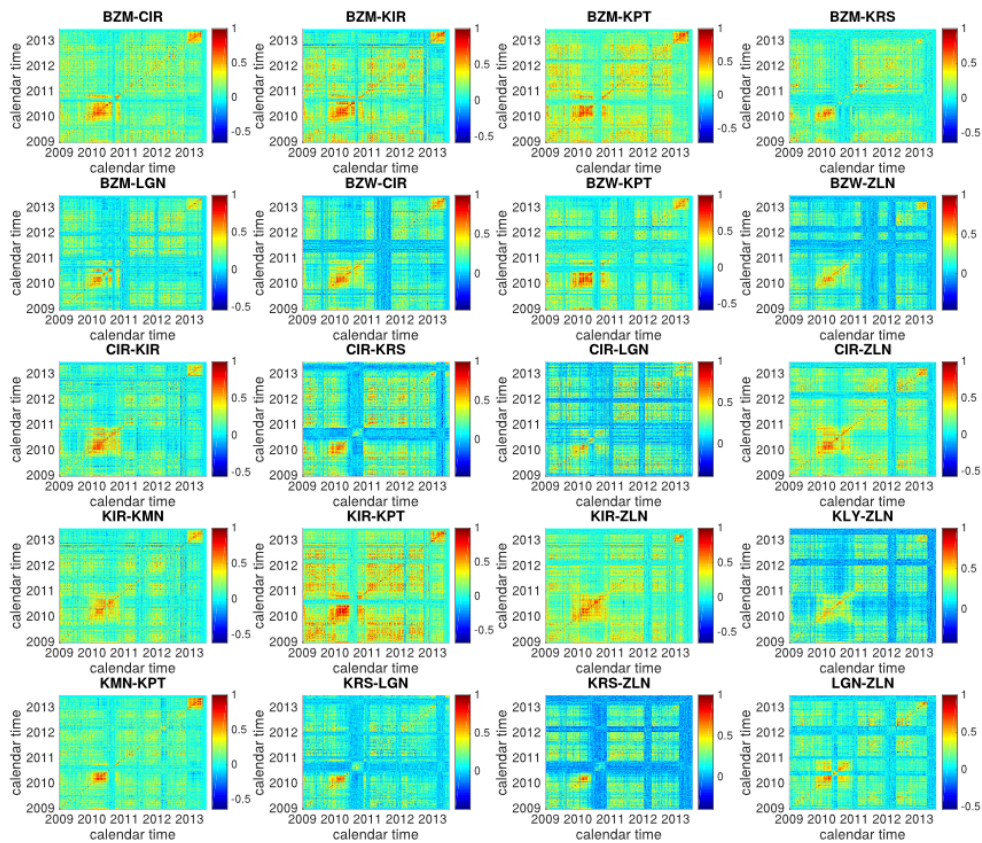


Figure 14. Correlation coefficient matrices between all daily CCF from January 2009 to August 2013 associated to 20 station pairs of group A located in the vicinity of Klyuchevskoy and Tolbachik volcanoes.

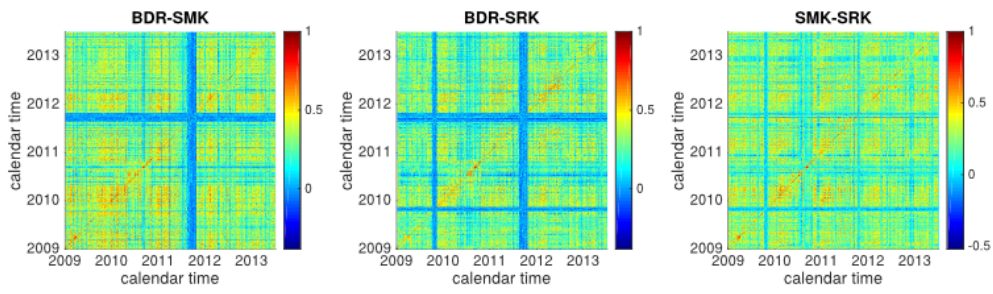


Figure 15. Correlation coefficient matrices between all daily CCF from January 2009 to August 2013 associated to the station pairs of group A located in the vicinity of Shiveluch.

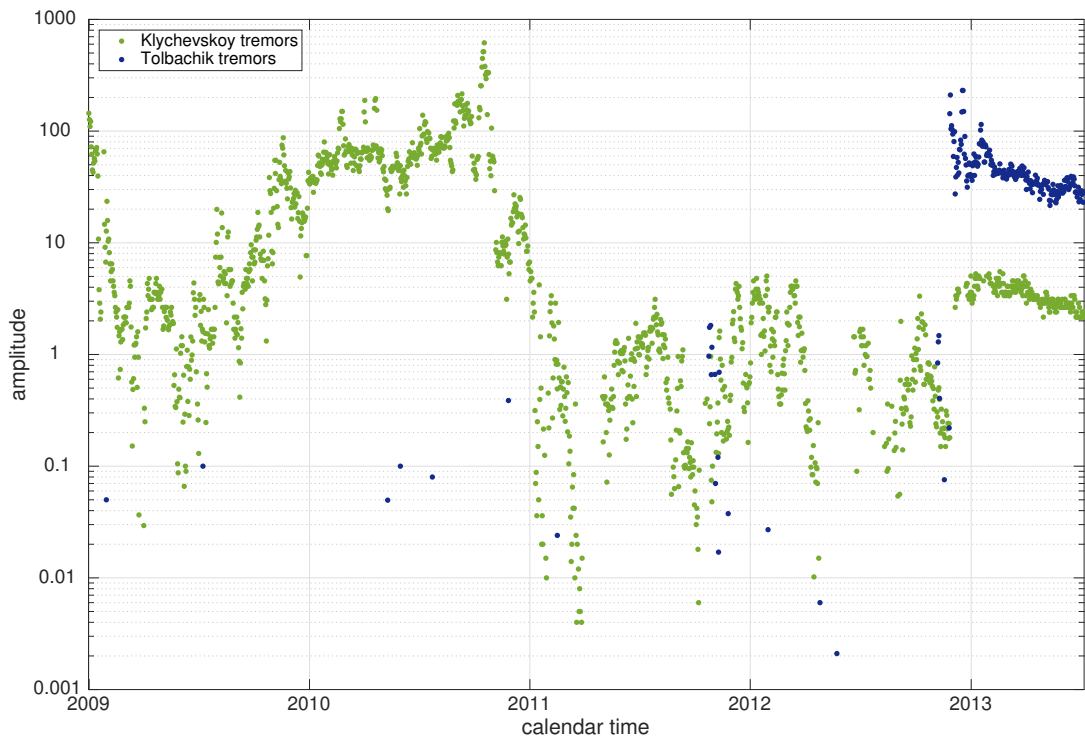


Figure 16. Normalized tremor amplitudes for Klychevskoy (green) and Tolbachik (blue) volcanoes.

4.3 Results

We show averaged velocity change time series reconstructed from CCFs of the quality group A. We average independently the stations near Shiveluch (3 station pairs) (Fig. 17) and the main group of station pairs (20 pairs in total) (Fig. 18) near Klyuchevskoy because the velocity changes associated with these two volcanoes can be very different. We compute raw relative velocity changes for all station pairs and average all curves. The parameters used for the inversion regularization are $\beta = 5$ and $\alpha = 100$. The mean coherence level of the CCFs considered in the inversion after rejecting correlation coefficients smaller than 0.3 (Figs 14 and 15), is 0.41 for both cases of averaged station pairs (3 station pairs near Shiveluch and 20 station pairs of the main group of stations).

To converge toward the actual relative velocity changes of the medium, we need to retrieve a stable trend due to long-term variations (LTV). We compute reconstructed velocity change time series from all considered station pairs with a large β value ($\beta = 1000$) to obtain precise velocity change curves that avoid short-term variations (STV). The value of the ponderation coefficient is the same than before, $\alpha = 100$. After obtaining all the individual LTV, we average them all to get the general trend.

We also plot the eruptive periods in the background of Figs 17 and 18, in green (Klyuchevskoy eruptions) and blue (Tolbachik eruption), overlaid with the reconstructed time series of velocity changes.

The maximum peak-to-peak amplitude of the retrieved LTV and the raw relative velocity changes, i.e., STV + LTV, is about 0.02 % (Fig. 18) which corresponds to the magnitude order of the amplitude of the expected velocity change curves used in sections 3.1 (Fig. 4a, expected velocity curve 3), 3.2 and 3.3. Regarding the inversion parameters, we use those tested in the synthetics: $\beta = 5$ for STV and $\beta = 1000$ for LTV. We keep the same ponderation coefficient for both cases: $\alpha = 100$. Comparing the results with the synthetics, for the mean coherence level obtained, 0.41, the correlation with the expected velocity change curve is 0.77 for long-term periodic-type fluctuations (Fig. 4b) while, for short-term fluctuations, $Q_{drop} = 0.67$ (Fig. 7). We can say that we achieve stable long and short-term variations with the averaged time series of velocity changes from 3 and 20 station pairs (Figs 17 and 18) since the mean coherence level of real CCFs for both cases ($coh = 0.41$) is greater than those in the synthetic averages of inverted time series of velocity changes over different station pairs (Figs 5a and 8a). Considering the uncertainties associated with the measurements, in case of seasonal variations, the correlation with the expected velocity curves of the reconstructed time series of velocity changes goes from 0.22 ± 0.28 , in case of one station pair used, to 0.38 ± 0.25 , averaging over 3 station pairs, and to 0.74 ± 0.10 with 20 station pairs (Fig. 5a). This means that, in cases of very low coh , the correlation increases by a factor between $\frac{0.38 - 0.25}{0.22 + 0.28} = 0.3$ and $\frac{0.38 + 0.25}{|0.22 - 0.28|} = 10.5$, averaging over 3 station

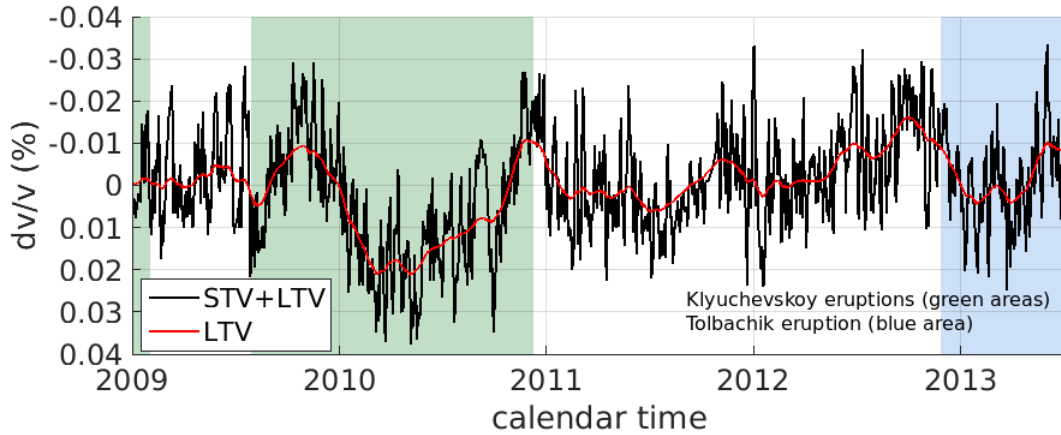


Figure 17. Evolution of relative velocity changes measured from three stations located near Shiveluch from January 2009 to August 2013. Raw relative velocity changes (STV+LTV in black) and long-term velocity variations (red curve) are overlaid. Klyuchevskoy and Tolbachik eruptions are shown with green and blue rectangles, respectively.

445 pairs, and between $\frac{0.74 - 0.10}{0.22 + 0.28} = 1.3$ and $\frac{0.74 + 0.10}{|0.22 - 0.28|} = 14$ with 20 station pairs. It is important
 446 to note that, for long-term and short-term variation, averaging over different pairs keeps these changes
 447 underestimated (Figs 5a and 8a) but the SNR increases by a factor of 1.6 when considering 3 station
 448 pairs instead of only one, and up to 2.5 with 20 station pairs (Fig. 8a). The increase of the SNR allows
 449 a better estimate of the timing of the abrupt velocity changes.

450 We also improve the ability of our method to recover velocity changes during the occurrence of
 451 low-frequency volcanic tremors by averaging different synthetic station pairs (Fig. 11a). Although
 452 there are high correlations between CCFs when high tremor activities take place (around 0.8 during
 453 2010 and 2013 periods in Figs 14 and 16), the mean coherence level of the CCFs used in the final in-
 454 version is low ($coh = 0.41$). Taking into account our synthetic results, in the situation of strong noise
 455 perturbations in the noise-correlation shape, when the correlations are highly unstable and, therefore,
 456 the coherence level is low, we need to average over enough station pairs. By averaging over 20 station
 457 pairs the correlation of the reconstructed time series of velocity changes with the expected velocity
 458 curve increases by a factor between 2.2 and 17.3, in regard to a single station pair (Fig. 11a). How-
 459 ever, we would retrieve more proper short to medium-term velocity changes due to episodic volcanic
 460 tremors by averaging over more than 40 station pairs, to interpret these velocity drops and retrievals
 461 without ambiguity (Fig. 11a).

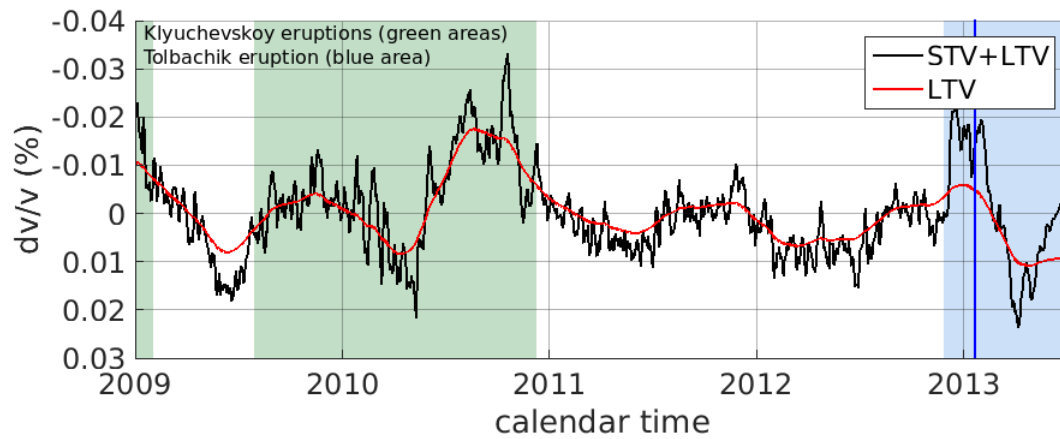


Figure 18. Evolution of relative velocity changes on Klyuchevskoy volcanic group from January 2009 to August 2013 (averaging of time series of velocity changes over 20 station pairs). Raw relative velocity changes (STV+LTV in black) and long-term velocity variations (red curve) are overlaid. Klyuchevskoy and Tolbachik eruptions are shown with green and blue rectangles, respectively.

462 5 INTERPRETATION OF THE RESULTS

463 The seismic velocity variations measured near Shiveluch (Fig. 15) are difficult to interpret because
 464 this measurement was done only with three station pairs and is, therefore very noisy. Besides, the
 465 measurements made with 20 station pairs surrounding the Klyuchevskoy group of volcanoes show
 466 velocity variations that can be interpreted in relationship of eruptive history of the two most active
 467 volcanoes of this group: Klyuchevskoy and Tolbachik. The whole velocity variations (STV+LTV) are
 468 controlled by the combination of two main mechanisms: by the variations of the media mechanical
 469 properties caused by the magma motion and pressurization within the volcano plumbing systems and
 470 by the environmental effects. These two mechanisms cannot be simply separated as STV and LTV
 471 computed during the data analysis because the long-duration eruptions of Klyuchevskoy and Tolbachik
 472 have their imprint on both STV and LTV.

473 The environmental contribution to the seismic velocity variations is expected to be controlled by
 474 seasonal changes in temperature, in hydrological loads, and in snow cover. These seasonal effects are
 475 particularly strong in Kamchatka and, therefore, we decided to estimate it and to remove from the
 476 whole time series, expecting that the remaining velocity variations mainly reflect the dynamics of the
 477 volcano plumbing system. To estimate the average long-term seasonal component from the velocity
 478 variation time series shown in Fig. 18, we computed median $\frac{dv}{v}$ values for every Julian day. Then,
 479 the obtained one-year periodic function has been smoothed in a 3-month long moving window. The
 480 resulted seasonal variations are shown with a thick gray line in Fig. 19a. The seasonality is very clear
 481 with a very pronounced velocity increase during winter (between end of December and end of April)
 482 and a pronounced velocity decrease during summer (between end of May and end of August).

483 After removing this seasonal trend, the velocity variations exhibit three significant periods with
 484 decrease over 0.01% (Fig 19b). The first of this velocity drops corresponds to the end of the 2008-2009
 485 Klyuchevskoy eruption. The second drop starts at the end of May 2010 and terminates simultaneously
 486 with the 2009-2010 Klyuchevskoy eruption. The third velocity decrease starts approximately simul-
 487 taneously with the 2012-2013 Tolbachik eruption. Therefore, all detected decreases in seismic veloc-
 488 ity are observed during eruptions and most likely reflect the inflation-caused dilation of the shallow
 489 crustal layers. Nevertheless, the durations of the observed velocity drops do not exactly coincide with
 490 the known periods of eruptive activity. A possible explanation for this is that during the long-duration
 491 of Kamchatka volcanoes, the state of the plumbing system exhibits significant changes.

492 The detailed source analysis of co-eruptive tremors by Soubestre et al. (2017) has identified two
 493 separate stages of activity during the 2009-2010 Klyuchevskoy eruption. The second stage that started
 494 approximately in May 2010 (indicated with vertical dashed line in Fig. 19b) was more intensive with
 495 magma likely moving closer to the surface. The observed velocity drop coincides in time with the

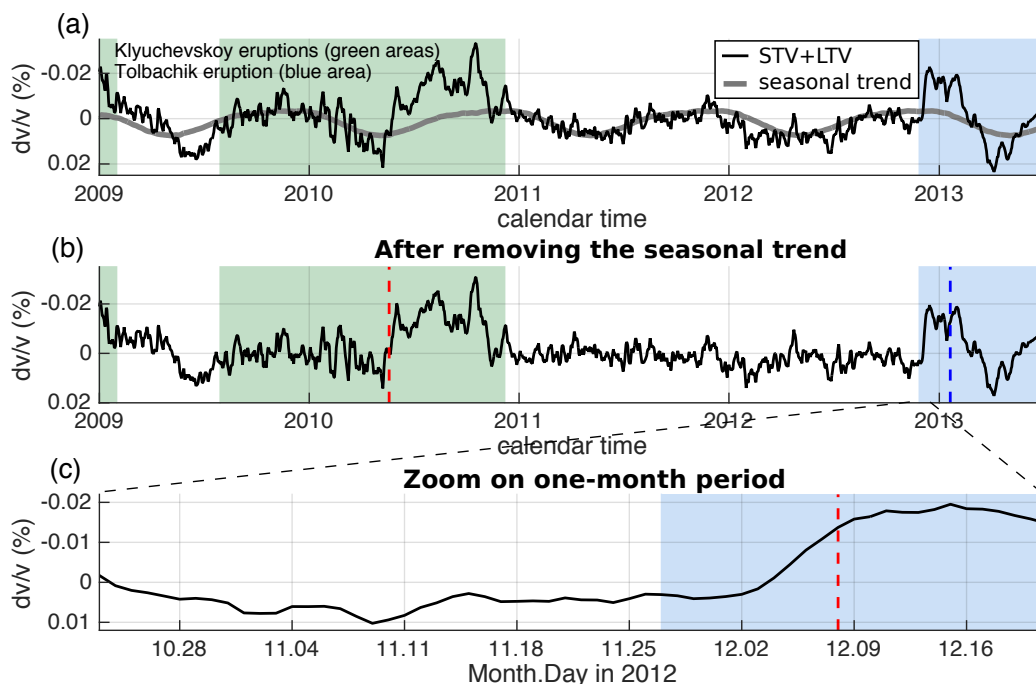


Figure 19. Evolution of relative velocity changes on Klyuchevskoy volcanic group from January 2009 to August 2013 (averaging of time series of velocity changes over 20 station pairs). (a) Raw relative velocity changes (in black) and average seasonal variations (thick gray curve) are overlaid. (b) Velocity variations after removing the seasonal component. Periods of the Klyuchevskoy and Tolbachik eruptions are shown with green rectangles, respectively. The vertical red dashed line indicates the onset of the second stage of the 2009-2010 Klyuchevskoy eruption (Soubestre et al. 2017). (c) Zoom on one-month period including the beginning of the Tolbachik eruption (green rectangle). The vertical red dashed line indicates the onset of the main eruption stage.

496 second stage and confirms that the large-scale magma migration occurred between the two stages of
 497 eruption.

498 The level of seismic velocity changes also strongly varied during the 2012-2013 Tolbachik erup-
 499 tion. We observe, in particular, that the onset of the strong velocity drop does not coincide with the
 500 beginning of the eruption (Fig. 19c) but rather with the beginning of its main stage when the out-
 501 pouring of lava concentrated in a single vent where the main eruptive Naboko cone started to grow
 502 (Belousov et al. 2015). The later variations in seismic velocities are consistent with changes in tremor
 503 sources identified based on correlations of continuous seismic records (Shapiro et al. 2017b).

504 **6 CONCLUSIONS**

505 To summarize, we classify the principal ideas of this work in three itemized sections, according to the
 506 methodology, the synthetic tests and the real data results.

507 • We have proposed a generalized formulation for retrieving continuous time series of velocity
 508 changes avoiding the definition of an arbitrary reference CCF.

509 – We measure seismic velocity changes between all possible pairs of daily CCFs applying the
 510 MWCS analysis.

511 – The final time series of velocity changes is obtained by inversion, using a classical Bayesian
 512 linear least square formulation. In the inversion, the role of α and β , the regularization parameters,
 513 is essential.

514 – After inverting, we sort STV and LTV. We retrieve LTV choosing a large β . We further com-
 515 pute STV subtracting the LTV from the raw relative velocity changes, obtained with a small β in
 516 the inversion.

517 • To check the reliability of our method, we computed synthetic tests with the aim of estimating
 518 the expected reliability of velocity temporal changes.

519 – To recover stable long-term periodic-type velocity variations produced by a seasonal-type
 520 trend, we use $\beta = 1000$ and consider different α , choosing lower values for low *coh* of the CCFs.
 521 We check the improvement associated with averaging over different receiver pairs even when the
 522 *coh* between daily cross-correlation functions is quite low.

523 – We reconstruct short-term velocity fluctuations (sudden velocity drops) as an effect of a sud-
 524 den change in the structure, such as an earthquake or a volcanic eruption. We use $\beta = 5$ and $\alpha \approx 0$
 525 in the inversion. Averaging over different station pairs, the sudden velocity changes remains under-
 526 estimated, however, the SNR of the reconstructed velocity series improves and, therefore, allows a
 527 better estimate of the timing of the velocity drop.

528 – We also test the ability of our method to retrieve short to medium-term velocity variations
 529 (rapid velocity drop and sudden recovery) due to the effect of a transient local source emission,
 530 such as a volcanic tremor. We use $\beta = 5$ and $\alpha \approx 0$ in the inversion. Our method produces
 531 artificial velocity drops in the situation of strong noise perturbations. In this cases, to retrieve
 532 proper velocity changes, we can (1) correct for the artificial baseline difference after inversion if
 533 the coherence level between CCFs is high or (2) average over sufficient station pairs when the
 534 coherence is low.

535 • We test and check the suitability and advantage of this approach by applying our method to the

536 Klyuchevskoy volcanic group dataset of noise cross-correlations, interfered with strong and localized
537 volcanic tremors and the lost of data.

538 – We compute averaged time series of velocity changes considering, independently, two group
539 of station pairs: 3 station pairs located in the vicinity of the Shiveluch volcano and 20 station pairs,
540 the main group of stations, in the KVG area. The parameters used in the inversion are $\beta = 5$ and
541 $\alpha = 100$ for raw relative velocity changes (STV+LTV) and $\beta = 1000$ and $\alpha = 100$ for LTV.

542 – For both groups of station pairs (near Shiveluch and the one in the KVG area), the mean
543 coherence level between CCFs is 0.41. The maximum peak-to-peak amplitude of the retrieved LTV
544 and the whole velocity variations (STV+LTV) is about 0.02 %. This allows us to compare with the
545 synthetics. Although short and long-term variations remain underestimated due to edge effects of
546 the time series, we achieve stable long and short-term variations averaging over the main group of
547 station pairs, 20 in total and the SNR increases. Therefore, we have a better estimate of the timing
548 of the abrupt short-term velocity changes. On the other hand, during the occurrence of volcanic
549 tremors we need to average over enough station pairs to ensure there are no artificial baselines,
550 since the coherence level between CCFs obtained from real data is low, 0.41. To interpret velocity
551 drops in these cases without ambiguity, it would be necessary to average over, at least, twice the
552 number of station pairs used (20 receiver pairs).

553 – STV and LTV cannot be separated in this particular case since long-term eruptions of Klyuchevskoy
554 and Tolbachik are controlled by the fluctuations of the media mechanical properties and by envi-
555 ronmental effects. After removing the seasonal trend, we observed three velocity decrease periods
556 over 0.01 % related with the inflation-caused dilation of the shallow crustal layers. The first de-
557 crease occurs at the end of the 2008-2009 Klyuchevskoy eruption, the second corresponds to the
558 second stage of the 2009-2010 Klyuchevskoy eruption Soubestre et al. (2017) and the third coin-
559 cides with the beginning of the main stage of the 2012-2013 Tolbachik eruption (Belousov et al.
560 2015). The duration of these velocity decrease periods does not exactly coincide with the eruptive
561 activity, probably because of the continuous and significant changes of the plumbing system in the
562 Kamchatka volcanoes.

563 We have established a general framework for this noise-based monitoring technique. Particular
564 care is required to recover temporal velocity variations from CCFs where the noise field recordings
565 are affected by transient tremor signals. In these cases, the processing to monitor active volcanoes
566 is critical. Although, here we use continuous noise-based seismic velocity change observations to
567 provide insights into volcanic unrest, this generalized formulation can be used as well to study crustal
568 earthquake relaxations and the effects of fluid injections in the sub-surface in cases where seismicity
569 interferes with the ambient seismic noise records.

570 **ACKNOWLEDGMENTS**

571 All the data used in this study were provided by the Kamchatka Branch of Geophysical Survey of
572 Russian Academy of Sciences (<http://www.emsd.ru>). This study was supported by REPSOL CO-DOS
573 project, by the European COST action TIDES (ES1401), by the Russian Science Foundation (grant
574 14-47-00002), by the French projects ‘Labex UnivEarth’ and Université Sorbonne Paris Cité project
575 ‘VolcanoDynamics’ by a research grant from Science Foundation Ireland (SFI) under Grant Number
576 13/RC/2092 and co-funded under the European Regional Development Fund and by iCRAG industry
577 partners. Computations were performed using the IPGP High-Performance Computing infrastructure
578 S-CAPADE (supported by the Île-de-France region via the SEASAME programme, by France-Grille,
579 and by the CNRS MASTODONS programme).

580 **REFERENCES**

- 581 Ballmer, S., Wolfe, C. J., Okubo, P. G., Haney, M. M., & Thurber, C. H., 2013. Ambient seismic noise interfer-
582 ometry in Hawai’i reveals long-range observability of volcanic tremor, *Geophysical Journal International*,
583 **194**(1), 512–523.
- 584 Belousov, A., Belousova, M., Edwards, B., Volynets, A., & Melnikov, D., 2015. Overview of the precursors
585 and dynamics of the 2012–13 basaltic fissure eruption of Tolbachik Volcano, Kamchatka, Russia, *Journal of*
586 *Volcanology and Geothermal Research*, **307**, 22–37.
- 587 Bensen, G. D., Ritzwoller, M. H., Barmin, M. P., Levshin, a. L., Lin, F., Moschetti, M. P., Shapiro, N. M., &
588 Yang, Y., 2007. Processing seismic ambient noise data to obtain reliable broad-band surface wave dispersion
589 measurements, *Geophysical Journal International*, **169**(3), 1239–1260.
- 590 Brenguier, F., Campillo, M., Hadziioannou, C., Shapiro, N., Nadeau, R. M., & Larose, E., 2008a. Postseismic
591 relaxation along the San Andreas fault at Parkfield from continuous seismological observations, *Science*,
592 **321**(5895), 1478–1481.
- 593 Brenguier, F., Shapiro, N. M., Campillo, M., Ferrazzini, V., Duputel, Z., Coutant, O., & Nercessian, A., 2008b.
594 Towards forecasting volcanic eruptions using seismic noise, *Nature Geoscience*, **1**(2), 126–130.
- 595 Brenguier, F., Campillo, M., Takeda, T., Aoki, Y., Shapiro, N. M., Briand, X., Emoto, K., & Miyake, H., 2014.
596 Mapping pressurized volcanic fluids from induced crustal seismic velocity drops, *Science*, **345**(July), 80–2.
- 597 Campillo, M., Sato, H., Shapiro, N. M., & Van Der Hilst, R. D., 2011. New developments on imaging and
598 monitoring with seismic noise, *Comptes Rendus Geoscience*, **343**(8-9), pp–487.
- 599 Caudron, C., Taisne, B., Kugaenko, Y., & Saltykov, V., 2015. Magma migration at the onset of the 2012–13
600 Tolbachik eruption revealed by Seismic Amplitude Ratio Analysis, *Journal of Volcanology and Geothermal*
601 *Research*, **307**, 60–67.
- 602 Chaves, E. J. & Schwartz, S. Y., 2016. Monitoring transient changes within overpressured regions of subduc-
603 tion zones using ambient seismic noise, *Science advances*, **2**(1), e1501289.

- 604 Chebrov, V. N., Droznin, D. V., Kugaenko, Y., Levina, V. I., Senyukov, S. L., Sergeev, V. A., Shevchenko,
605 Y., & Yashchuk, V. V., 2013. The system of detailed seismological observations in Kamchatka in 2011, *J.*
606 *Volcanol. Seismol.*, **7**(1), 16–36.
- 607 Chouet, B. A., 1996. Long-period volcano seismicity: its source and use in eruption forecasting, *Nature*,
608 **380**(6572), 309.
- 609 Clarke, D., Zaccarelli, L., Shapiro, N. M., & Brenguier, F., 2011. Assessment of resolution and accuracy of the
610 Moving Window Cross Spectral technique for monitoring crustal temporal variations using ambient seismic
611 noise, *Geophysical Journal International*, **186**(2), 867–882.
- 612 Colombi, A., Chaput, J., Brenguier, F., Hillers, G., Roux, P., & Campillo, M., 2014. On the temporal stability
613 of the coda of ambient noise correlations, *Comptes Rendus - Geoscience*, **346**(11-12), 307–316.
- 614 Dorendorf, F., Wiechert, U., & Wörner, G., 2000. Hydrated sub-arc mantle: a source for the Klyuchevskoy
615 volcano, Kamchatka/Russia, *Earth Planet. Sci. Lett.*, **175**(1), 69–86.
- 616 Droznin, D. V., Shapiro, N. M., Droznina, S. Y., Senyukov, S. L., Chebrov, V. N., & Gordeev, E. I., 2015.
617 Detecting and locating volcanic tremors on the Klyuchevskoy group of volcanoes (Kamchatka) based on
618 correlations of continuous seismic records, *Geophysical Journal International*, **203**(2), 1001–1010.
- 619 Duputel, Z., Ferrazzini, V., Brenguier, F., Shapiro, N., Campillo, M., & Nercessian, A., 2009. Real time
620 monitoring of relative velocity changes using ambient seismic noise at the Piton de la Fournaise volcano
621 (La Réunion) from January 2006 to June 2007, *Journal of Volcanology and Geothermal Research*, **184**(1),
622 164–173.
- 623 Fedotov, S. A., Khrenov, A. P., & Jarinov, N. A., 1987. Klyuchevskoy volcano, its activity in 1932–1986 and
624 possible development, *Volcanol. Seism.*, **4**, 3–16.
- 625 Gordeev, E., Murav'ev, Y., Samoilenko, S., Volynets, A., Mel'nikov, D., & Dvigalo, V. N., 2013. The Tolbachik
626 fissure eruption of 2012–2013: Preliminary results, *Dokl. Earth Sci.*, **452**(2), 1046–1050.
- 627 Gordeev, E. I., Saltykov, V. A., Sinitsyn, V. I., & Chebrov, V. N., 1990. Temporal and spatial characteristics of
628 volcanic tremor wave fields, *Journal of Volcanology and Geothermal Research*, **40**(1), 89–101.
- 629 Hadziioannou, C., Larose, E., Coutant, O., Roux, P., & Campillo, M., 2009. Stability of monitoring weak
630 changes in multiply scattering media with ambient noise correlation: laboratory experiments., *J. Acoust. Soc.*
631 *Am.*, **125**(6), 3688–3695.
- 632 Hillers, G., Husen, S., Obermann, A., Planès, T., Larose, E., & Campillo, M., 2015. Noise-based monitoring
633 and imaging of aseismic transient deformation induced by the 2006 Basel reservoir stimulation, *Geophysics*,
634 **80**(4), KS51–KS68.
- 635 Hobiger, M., Wegler, U., Shiomi, K., & Nakahara, H., 2012. Coseismic and postseismic elastic wave velocity
636 variations caused by the 2008 Iwate-Miyagi Nairiku earthquake, Japan, *Journal of Geophysical Research:*
637 *Solid Earth*, **117**(B9).
- 638 Koulakov, I., Gordeev, E. I., Dobretsov, N. L., Vernikovskiy, V. A., Senyukov, S., Jakovlev, A., & Jaxybulatov,
639 K., 2013. Rapid changes in magma storage beneath the Klyuchevskoy group of volcanoes inferred from
640 time-dependent seismic tomography, *Journal of Volcanology and Geothermal Research*, **263**, 75–91.

- 641 Larose, E., Margerin, L., Derode, A., van Tiggelen, B., Campillo, M., Shapiro, N., Paul, A., Stehly, L., &
642 Tanter, M., 2006. Correlation of random wavefields: An interdisciplinary review, *Geophysics*, **71**(4), SI11–
643 SI21.
- 644 Lees, J. M., Symons, N., Chubarova, O., Gorelichik, V., & Ozerov, A., 2013. Tomographic Images of
645 Klyuchevskoy Volcano P-Wave Velocity, in *Volcanism Subduction Kamchatka Reg.*, pp. 293–302.
- 646 Levin, V., Shapiro, N., Park, J., & Ritzwoller, M., 2002. Seismic evidence for catastrophic slab loss beneath
647 Kamchatka, *Nature*, **418**(6899), 763.
- 648 Levin, V., Shapiro, N. M., Park, J., & Ritzwoller, M. H., 2005. Slab portal beneath the western Aleutians,
649 *Geology*, **33**(4), 253–256.
- 650 Meier, U., Shapiro, N. M., & Brenguier, F., 2010. Detecting seasonal variations in seismic velocities within
651 Los Angeles basin from correlations of ambient seismic noise, *Geophysical Journal International*, **181**(2),
652 985–996.
- 653 Mordret, A., Jolly, A., Duputel, Z., & Fournier, N., 2010. Monitoring of phreatic eruptions using interferometry
654 on retrieved cross-correlation function from ambient seismic noise: Results from Mt. Ruapehu, New Zealand,
655 *Journal of Volcanology and Geothermal Research*, **191**(1), 46–59.
- 656 Nikulin, A., Levin, V., Shuler, A., & West, M., 2010. Anomalous seismic structure beneath the Klyuchevskoy
657 Group, Kamchatka, *Geophysical Research Letters*, **37**(14).
- 658 Niu, F., Silver, P. G., Daley, T. M., Cheng, X., & Majer, E. L., 2008. Preseismic velocity changes observed
659 from active source monitoring at the Parkfield SAFOD drill site, *Nature*, **454**(7201), 204.
- 660 Obermann, A., Planes, T., Larose, E., & Campillo, M., 2013. Imaging preruptive and coeruptive structural
661 and mechanical changes of a volcano with ambient seismic noise, *Journal of Geophysical Research: Solid*
662 *Earth*, **118**(12), 6285–6294.
- 663 Ozerov, A. Y., Firstov, P. P., & Gavrilov, V. A., 2013. Periodicities in the Dynamics of Eruptions of
664 Klyuchevskoi Volcano, Kamchatka, in *Volcanism Subduction Kamchatka Reg.*, pp. 283–291.
- 665 Poupinet, G., Ellsworth, W. L., & Frechet, J., 1984. Monitoring velocity variations in the crust using earthquake
666 doublets: An application to the Calaveras Fault, California, *Journal of Geophysical Research: Solid Earth*,
667 **89**(B7), 5719.
- 668 Rivet, D., Brenguier, F., Clarke, D., Shapiro, N. M., & Peltier, A., 2014. Long-term dynamics of Piton de la
669 Fournaise volcano from 13 years of seismic velocity change measurements and GPS observations, *Journal*
670 *of Geophysical Research: Solid Earth*, **119**(10), 7654–7666.
- 671 Roux, P., Sabra, K. G., Gerstoft, P., Kuperman, W. A., & Fehler, M. C., 2005. P-waves from cross-correlation
672 of seismic noise, *Geophysical Research Letters*, **32**(19), 1–4.
- 673 Schaff, D. P., 2012. Placing an upper bound on preseismic velocity changes measured by ambient noise
674 monitoring for the 2004 Mw 6.0 Parkfield earthquake (California), *Bulletin of the Seismological Society of*
675 *America*, **102**(4), 1400–1416.
- 676 Schneider, D., Dean, K., Dehn, J., Miller, T., Kirianov, V. Y., et al., 2000. Monitoring and analyses of volcanic
677 activity using remote sensing data at the Alaska Volcano Observatory: case study for Kamchatka, Russia,

- 678 December 1997, *Remote Sensing of Active Volcanism*, pp. 65–85.
- 679 Sens-Schönfelder, C. & Wegler, U., 2006. Passive image interferometry and seasonal variations of seismic
680 velocities at Merapi Volcano, Indonesia, *Geophysical Research Letters*, **33**(21), 1–5.
- 681 Sens-Schönfelder, C., Pomponi, E., & Peltier, A., 2014. Dynamics of Piton de la Fournaise volcano observed
682 by passive image interferometry with multiple references, *Journal of Volcanology and Geothermal Research*,
683 **276**, 32–45.
- 684 Senyukov, S. L., 2013. Monitoring and prediction of volcanic activity in Kamchatka from seismological data:
685 2000–2010, *J. Volcanol. Seismol.*, **7**(1), 86–97.
- 686 Senyukov, S. L., Droznina, S. Y., Nuzhdina, I. N., Garbuzova, V. T., & Kozhevnikova, T. Y., 2009. Studies
687 in the activity of Klyuchevskoi volcano by remote sensing techniques between January 1, 2001 and July 31,
688 2005, *J. Volcanol. Seismol.*, **3**(3), 191–199.
- 689 Shapiro, N. M. & Campillo, M., 2004. Emergence of broadband Rayleigh waves from correlations of the
690 ambient seismic noise, *Geophysical Research Letters*, **31**(7).
- 691 Shapiro, N. M., Campillo, M., Stehly, L., & Ritzwoller, M. H., 2005. High-resolution surface-wave tomogra-
692 phy from ambient seismic noise, *Science*, **307**(5715), 1615–1618.
- 693 Shapiro, N. M., Ritzwoller, M., & Bensen, G., 2006. Source location of the 26 sec microseism from cross-
694 correlations of ambient seismic noise, *Geophysical Research Letters*, **33**(18).
- 695 Shapiro, N. M., Droznin, D., Droznina, S. Y., Senyukov, S., Gusev, A., & Gordeev, E., 2017a. Deep and shallow
696 long-period volcanic seismicity linked by fluid-pressure transfer, *Nature Geoscience*, **10**(6), 442–445.
- 697 Shapiro, N. M., Droznin, D., Droznina, S. Y., Senyukov, S., Gusev, A., & Gordeev, E., 2017b. Variations
698 of properties of seismic tremor during the 2012-2013 eruption of the Tolbachik volcano based on correla-
699 tions of continuous seismic records in the Tolbachik fissure eruption of 2012-2013: results of investigations,
700 probability model, role for understanding of basalt eruption in subduction zones, in press (in Russian).
- 701 Slavina, L. B., Pivovarova, N. B., & Senyukov, S. L., 2012. Velocity structure of the crust and upper mantle at
702 the northern group of Kamchatka volcanoes (Based on the travel time of P-waves from volcanic earthquakes),
703 *Izv. Atmos. Ocean. Phys.*, **48**(7), 696–705.
- 704 Soubestre, J., Shapiro, N., Seydoux, L., de Rosny, D., Droznina, S., Senyukov, S., & Gordeev, E., 2017.
705 Network-based detection and classification of seismo-volcanic tremors: example from the Klyuchevskoy
706 volcanic group in Kamchatka, Manuscript submitted for publication.
- 707 Stehly, L., Froment, B., Campillo, M., Liu, Q. Y., & Chen, J. H., 2015. Monitoring seismic wave velocity
708 changes associated with the Mw 7.9 Wenchuan earthquake: increasing the temporal resolution using curvelet
709 filters, *Geophysical Journal International*, **201**(3), 1939–1949.
- 710 Tarantola, A., 2005. *Inverse problem theory and methods for model parameter estimation*, SIAM.
- 711 Ugalde, A., Villaseñor, A., Gaité, B., Casquero, S., Martí, D., Calahorrano, A., Marzán, I., & Carbonell, R.,
712 2013. Passive seismic monitoring of an experimental CO₂ geological storage site in Hontomín, *Seismological
713 Research Letters*, **84**(1), 75–84.
- 714 Ugalde, A., Gaité, B., & Villaseñor, A., 2014. Temporal variations of seismic velocity at Paradox Valley,

- 715 Colorado, using passive image interferometry, *Bulletin of the Seismological Society of America*, **104**(3),
716 1088–1099.
- 717 Wapenaar, K. & Fokkema, J., 2006. Green's function representations for seismic interferometry, *Geophysics*,
718 **71**(4), SI33–SI46.
- 719 Wapenaar, K., Draganov, D., Snieder, R., Campman, X., & Verdel, A., 2010. Tutorial on seismic interferome-
720 try: Part 1—Basic principles and applications, *Geophysics*, **75**(5), 75A195–75A209.
- 721 Wegler, U. & Sens-Schönfelder, C., 2007. Fault zone monitoring with passive image interferometry, *Geophys-*
722 *ical Journal International*, **168**(3), 1029–1033.
- 723 Yogodzinski, G. M., Lees, J. M., Churikova, T. G., Dorendorf, F., Wöerner, G., & Volynets, O. N., 2001.
724 Geochemical evidence for the melting of subducting oceanic lithosphere at plate edges, *Nature*, **409**(January),
725 500–504.
- 726 Zharinov, N. A. & Demyanchuk, Y. V., 2009. The February – July 2007 Eruption of the Summit Crater of
727 Klyuchevskoi Volcano, Kamchatka, *J. Volcanol. Seismol.*, **3**(3), 179–190.
- 728 Zhou, R., Huang, L., Rutledge, J. T., Fehler, M., Daley, T. M., & Majer, E. L., 2010. Coda-wave interferometry
729 analysis of time-lapse VSP data for monitoring geological carbon sequestration, *International Journal of*
730 *Greenhouse Gas Control*, **4**(4), 679–686.